



INTERNATIONAL UNIVERSITY LIAISON INDONESIA (IULI)

BACHELOR'S THESIS

---

A STUDY OF LAMINAR-TURBULENT TRANSITION ON  
TWO-DIMENSIONAL SUCTION BOUNDARY LAYER

---

By

**Lutfi Muzzaki Khairullah**

11201501009

Presented to the Faculty of Engineering  
In Partial Fulfilment Of the Requirements for the Degree of

SARJANA TEKNIK

In

AVIATION ENGINEERING

FACULTY OF ENGINEERING

BSD City 15345

Indonesia

August 2020

## APPROVAL PAGE

### A STUDY OF LAMINAR-TURBULENT TRANSITION ON TWO-DIMENSIONAL SUCTION BOUNDARY LAYER

LUTFI MUZZAKI KHAIRULLAH

11201501009

Presented to the Faculty of Engineering

In Partial Fulfillment of the Requirements for the Degree of

SARJANA TEKNIK

In

AVIATION ENGINEERING

FACULTY OF ENGINEERING

Dr. Eng. Ressa Octavianty

Thesis Advisor

\_\_\_\_\_

Date

Triwanto Simanjuntak, PhD

Thesis Co-Advisor

\_\_\_\_\_

Date

Dr. Ir. Prianggada Indra Tanaya, M.M.E.

Dean of Faculty of Engineering

\_\_\_\_\_

Date

## STATEMENT BY THE AUTHOR

I hereby declare that this submission is my own work and to the best of my knowledge, it contains no material previously published or written by another person, nor material which to a substantial extent has been accepted for the award of any other degree or diploma at any educational institution, except where due acknowledgement is made in the thesis.

Lutfi Muzzaki Khairullah

Student

Date

## ABSTRACT

A Study of Laminar-Turbulent Transition on Two-Dimensional Suction Boundary  
Layer

by

Lutfi Muzzaki Khairullah

Dr. Eng. Ressa Octavianty, Advisor

Triwanto Simanjuntak, PhD, Co-Advisor

In this thesis, the temporal stability of two-dimensional asymptotic suction flow was studied at wide-range of Reynolds number. Linear stability with small disturbances were introduced to Navier-Stokes equations in viscous boundary layer flow, in the form of Orr-Sommerfeld equation. Here, the compressibility effect was neglected in the assumption. A spectral collocation method was used to solve the fourth-order ordinary differential equation (ODE) of generalized eigenvalues problem. MATLAB and Python softwares were used to perform the numerical calculation. Moreover, this thesis benefits the highly accurate and widely used open-source function-based numerical computing system, i.e. Chebfun. Two variables were varied, Reynolds number  $Re$  and wavenumber  $\alpha$  to investigate the temporal growth of disturbances in this flow. Note that in this study, Reynolds number was from  $10^3$  to  $10^8$ , and  $\alpha$  was in the range of 0.01 to 0.30. It was found that both variables indeed affect the temporal stability where the flow is stable for all alphas at  $Re <$  than  $Re$  critical ( $Re_{crit} = 48\,000$ ). It should be noted also that for wide range of Reynolds numbers, no temporal growth appeared at  $\alpha > 0.19$ . In addition, the highest growth was observed at  $198\,155 < Re < 500\,566$ , for all wavenumbers within range of 0.1 – 0.12. With the limitaton of machine and high computational cost, the accuracy of the results is in order of  $\mathcal{O}(10^3)$  for the Reynolds number and  $\mathcal{O}(10^{-2})$  for the wavenumber  $\alpha$ .

Keyword: *Orr-Sommerfeld Equation, Boundary Layer, Spectral Collocation Method, Stability, Transition, Laminar, Turbulent, Suction*

## ACKNOWLEDGEMENTS

All praises to Allah The Most Beneficent and The Most Merciful for the accomplishment of this thesis. I thank God for all the opportunities, trials and strength that have been showered on me to finish writing the thesis. I experienced so much during this process, not only from the academic aspect but also from the aspect of personality. My humblest gratitude to the holy Prophet Muhammad (Peace be upon him) whose way of life has been a continuous guidance for me.

During the process of this thesis, I have gained a huge amount of assistances and supports. I would like to sincerely thank my beloved thesis advisor, Dr. Eng. Ressa Octaviany, and my thesis co-advisor, Triwanto Simanjuntak, PhD, for their patience, understanding and positive motivation.

My deepest gratitude goes to all of my family members. I would like to thank my father, mother and my sister for their support in almost every aspect.

I would like to extend my thanks to Gede, Jason, Joshua, Kiki (Rizki), Bagas, Jordy and all of my family members of Aviation Engineering 2015 for all the support and positive environment.

Last but not least, for everyone that I have not mentioned yet.

May God shower the above cited with all the blessings in their life.

# Contents

<b>Approval Page</b>	<b>i</b>
<b>Statement by The Author</b>	<b>ii</b>
<b>Abstract</b>	<b>iii</b>
<b>Acknowledgements</b>	<b>iv</b>
<b>Contents</b>	<b>v</b>
<b>List of Figures</b>	<b>viii</b>
<b>1 Introduction</b>	<b>1</b>
1.1 General Statement of Problem Area . . . . .	1
1.2 Research Purpose . . . . .	5
1.3 Significance of the Study . . . . .	5
1.4 Theoretical Perspective . . . . .	6
1.5 Research Scope and Limitation . . . . .	7
1.6 Methodology . . . . .	8
1.7 Design and Instrumentation . . . . .	8
1.8 Data Analysis . . . . .	8
<b>2 Literature Review</b>	<b>9</b>
2.1 Introduction to Boundary Layer . . . . .	9
2.1.1 Boundary Layer Properties . . . . .	10
2.1.2 Laminar and Turbulent Boundary Layer . . . . .	12
2.2 Laminar to Turbulent Transition of Boundary Layer . . . . .	15
2.2.1 The Transition Process . . . . .	15

2.2.2	Classification of Transition Process . . . . .	16
2.2.3	Important Parameters that Affect Laminar to Turbulent Transition . . . . .	18
2.3	Theory of Stability . . . . .	19
2.3.1	The General Concept of Stability . . . . .	20
2.3.2	Inviscid-Stability Theory . . . . .	20
2.3.3	Viscous-Stability Theory . . . . .	21
2.4	Governing Equations . . . . .	22
2.4.1	Navier-Stokes Equation . . . . .	22
2.4.2	Conservation of Mass . . . . .	23
2.4.3	Conservation of Momentum . . . . .	23
2.4.4	Orr-Sommerfeld Equation . . . . .	25
2.5	Spectral Collocation Methods . . . . .	29
2.5.1	Smoothness and Spectral Accuracy . . . . .	30
2.5.2	Eigenvalues and Fourth-Order Problems . . . . .	31
<b>3</b>	<b>Research Methodology</b>	<b>33</b>
3.1	Introduction to the Method . . . . .	33
3.1.1	Spectral Methods . . . . .	33
3.1.2	Eigenvalue and Generalized Eigenvalue Problems . . . . .	33
3.1.3	Spectral Collocation Methods of Asymptotic Suction Boundary Layer . . . . .	34
3.2	Computing Tools . . . . .	36
3.2.1	Chebfun Codes for MATLAB . . . . .	36
3.2.2	MATLAB and Python . . . . .	37
3.2.3	MATLAB Engine API for Python . . . . .	39
3.3	Variables . . . . .	39
3.4	Prediction of Temporal Stability . . . . .	40
<b>4</b>	<b>Results and Discussions</b>	<b>41</b>
4.1	Computation Variables . . . . .	41
4.2	Data Plot for Several Wavenumbers . . . . .	42
4.2.1	Data Plot for Wavenumber 0.01 . . . . .	42
4.2.2	Data Plot for Wavenumber 0.15 . . . . .	43

4.2.3	Data Plot for Wavenumber 0.24 . . . . .	44
4.2.4	Data Plot for All Wavenumbers . . . . .	46
4.3	Stability Analysis at Complex Plane . . . . .	46
4.3.1	Stable State . . . . .	46
4.3.2	Unstable Condition . . . . .	49
4.4	The Contour of Stability . . . . .	49
4.4.1	Contour Plot of The Data . . . . .	49
4.4.2	Comparison . . . . .	51
<b>5</b>	<b>Summary, Conclusion, Recommendation</b>	<b>52</b>
5.1	Conclusions . . . . .	52
5.2	Remarks for the Future Work . . . . .	53
	<b>References</b>	<b>54</b>
	<b>Appendices</b>	<b>56</b>
	<b>Appendix A MATLAB and Python Codes</b>	<b>57</b>
A.1	Generalized Eigenvalue Problems (MATLAB) . . . . .	57
A.2	Wavenumber Data (Python) . . . . .	57
A.3	Plot Each Wavenumber (Python) . . . . .	59
A.4	Plot Each Wavenumber (Python) . . . . .	60
	<b>Appendix B Eigenvalues Data</b>	<b>63</b>
B.1	Alpha = 0.01 . . . . .	63
	<b>Turnitin Report</b>	<b>66</b>
	<b>Curriculum Vitae</b>	<b>79</b>

# List of Figures

1.1	Laminar to turbulent transition from a smoke . . . . .	2
1.2	Transition mechanism . . . . .	3
1.3	Visualization of different transition mechanisms . . . . .	4
1.4	Velocity profile of Blasius and turbulent boundary layers . . . . .	4
2.1	Boundary layer . . . . .	10
2.2	Mass conservation . . . . .	12
2.3	Displacement thickness . . . . .	13
2.4	Laminar to turbulent profile . . . . .	14
2.5	Laminar to turbulent transition . . . . .	14
2.6	The classis pipe-flow sye experiment . . . . .	15
2.7	Boundary layer transition process . . . . .	17
2.8	Smoke-flow visualization of transition flow . . . . .	18
2.9	Relative stability of a ball at rest . . . . .	19
2.10	Neutral curves of O-S equation . . . . .	22
2.11	Notation for stresses . . . . .	24
3.1	MATLAB Engine API for Python work process . . . . .	39
4.1	Data Plot for Alpha = 0.01 . . . . .	43
4.2	Data Plot for Alpha = 0.15 . . . . .	44
4.3	Data Plot for Alpha = 0.24 . . . . .	45
4.4	Data Plot for All Wavenumbers . . . . .	47
4.5	Eigenvalues at First Pair of Reynolds number and Wavenumber . . . . .	48
4.6	Eigenvalues at Second Pair of Reynolds number and Wavenumber . . . . .	49
4.7	The Contour Plot of Neutral Stability for A Viscous Flow . . . . .	50
4.8	The Contour Plot of Neutral Stability from Hughes and Reid . . . . .	51

A STUDY OF LAMINAR-TURBULENT TRANSITION ON TWO-DIMENSIONAL  
SUCTION BOUNDARY LAYER

---

*Dedicated to my parents*

# CHAPTER 1

## INTRODUCTION

### 1.1 General Statement of Problem Area

A flow condition is one of variables in fluid that enormously affects its quality. This condition assuredly applies for both inner and outer flow through a body. On its application, the body must be adjusted in order to make the initial flow condition could achieve the desired output.

A streamlined and smooth flow is the primary characteristic of laminar flow. The flow streams without obstruction, and any swirls or cross currents do not exist along the line of the flow. Although the layers are not crossing and intersecting each other, the fluid layers will still flow at different speeds. The center layer has the fastest flow speed while slower speed occurred with the increasing distance from the center of the flow. Laminar flow usually occurred at low  $Re$ .

Regardless of the fact that laminar flow is worthwhile to reduce drag production on the wing surface, the characteristic of the wing may not withstand much laminar flow. The North American P-51 Mustang was the former aircraft which purposely conceived to take advantage of laminar flow airfoils. Nevertheless, wartime investigation data of National Advisory Committee for Aeronautics (NACA) indicates that Mustangs were not designed to retain superior laminar flow on the wing with adequate surface performance (*Laminar Flow Airfoil*, 2015).

Notwithstanding, turbulent flow (usually occurred at high  $Re$ ) is a flow which its particles move randomly and chaotically. Numerous layers mix with each other and a huge amount of friction is appeared between the boundaries of the different layers. Eddies and whirlpools are produced within the flow. A significant transfer of energy, mass and momentum are consisted in turbulent flow. The flow will remains turbulent and irregular as long as the energy prevails. The flow returns back to laminar state whenever the energy is totally conserved (Nelson, 2018).



FIGURE 1.1: Laminar to turbulent transition from a smoke cigarette  
(*Courtesy of flickr*)

Turbulent flow is still not numerically well established in fluid dynamics. A simple instance of a transition phenomena can be found on a smoke from a cigarette, as shown in Figure 1.1. At first, the flow streams laminarly. Due to the presence of the disturbance on its surroundings, the flow then become turbulent. Although turbulence can be experimentally examined in wind tunnels and modeled numerically, most of the turbulent flow behavior remains uncertain. Studying the turbulent behavior, the turbulent boundary layer in particular, can provide insight into turbulence control and how to reduce the drag of the surface friction in various technical applications (Spaulding, 2019).

Transition flow is a mixture of both flows (intermittent fluctuation). This flow never occurs if  $Re < Re_{crit}$ . For streamline body, postponing or delaying the transition may reduce the production of pressure drag.

A laminar boundary layer can be destabilized by many factors that cause it to become turbulent. Examples of destabilizing effects include surface roughness, adverse pressure gradients, acoustic and heat energy. The growth of skin friction is the significant outcome of a chaotic boundary layer once it is transitioned. To sustain a laminar stream, a favorable pressure gradient is required. A large portion of prosperous pressure gradients is substantial for laminar flow airfoils. The common definition of the airfoil's laminar flow is that the desired pressure gradient

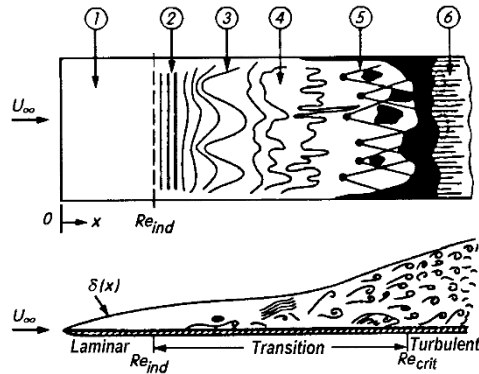


FIGURE 1.2: Various transition mechanism in boundary layer flow  
 (Schlichting & Gersten, 2016)

culminates between 30% and 75% of the chord.

As shown in Figure 1.2, transition mechanism can be categorized as stable laminar flow; unstable TollmienSchlichting (TS) waves; three-dimensional waves and vortex formation ( $\Lambda$ -structures); vortex decay; formation of turbulent spots; and fully turbulent flow.

The prediction of  $Re_{crit}$  is challenging as it is highly dependent on intensity of disturbance ( $u'$ ). Figure 1.3a, 1.3b and 1.3c show different process of transition for 0.2%, 0.3% and 0.4% freestream disturbances ( $u'$ ), respectively. For small disturbance, linear stability theory can accurately predict the  $Re_{crit}$ . The condition is stable if there is tendency to return to initial condition, no growth in disturbance. A more comprehensive explanation about linear stability theory will be explained later in Chapter 2.

Figure 1.4 shows a velocity profile of Blasius and turbulent boundary layers. By linear stability theory, the  $Re_{crit}$  of spatio-temporal stability is predicted at 520. From this case, arise one question, is it possible to increase the crit Re with flow control?

The importance of the study of laminar to turbulent transition brings up the topic to be remarkably necessary to be discussed since the transition affects quite significant in aerospace engineering applications. The transition affects the performance of an aircraft, such as range, which leads to a specific fuel consumption. Also, it impacts the aerodynamics quantity, e.g., drag and heat pulse. Another consequence is on the aircraft moment.

A STUDY OF LAMINAR-TURBULENT TRANSITION ON TWO-DIMENSIONAL SUCTION BOUNDARY LAYER

---

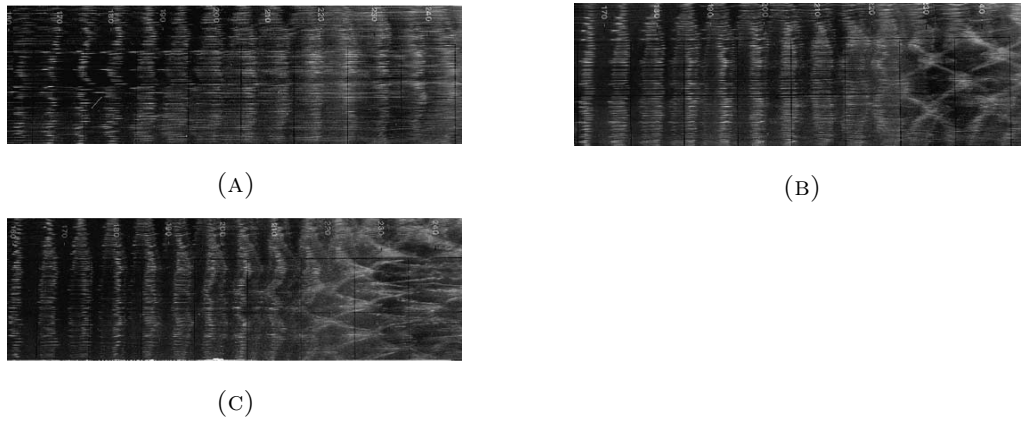


FIGURE 1.3: Visualization of different transition mechanisms (Saric, 1986)

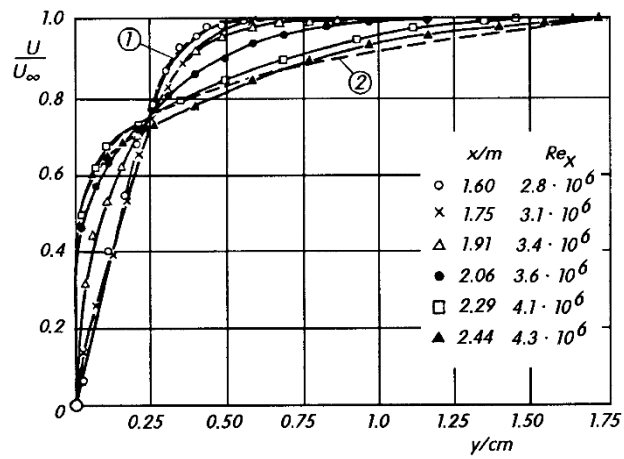


FIGURE 1.4: Velocity profile of Blasius (1) and turbulent (2) boundary layers

Suction is widely used to control the flow. The velocity profile of boundary layer with suction can be written as:

$$U/U_\infty = 1 - e^{y v_w / \nu} \quad (1.1)$$

where  $v_w$  is the suction velocity,  $\nu$  is dynamic viscosity.

As briefly explain in the background, it is necessary to investigate the transition of controlled boundary layer (suction), i.e. temporal stability analysis using linear stability theory.

## 1.2 Research Purpose

The objectives of this research are:

- To derive the Orr-Sommerfeld Equation for a 2D streamline body for a certain base flow.
- To build a numerical tool to solve the Orr-Sommerfeld Equation.
- To predict laminar-turbulent transition (Recrit) in terms of temporal stability and disturbance growth of suction boundary layer.
- To compare the results with other studies.

## 1.3 Significance of the Study

The results of this research are expected:

- The solution can be used to understand the mechanism and behavior of the transition flow on a 2D streamline body.
- It can be used to predict the disturbance growth and stability on the boundary layer.
- The understanding can be used to control the boundary layer development and drag reduction.

- The possibility of controlling the boundary layer above the surface may support aerospace industries to optimize the performance of aircrafts since laminar flow provides much lower-skin friction drag than turbulent flow.

## 1.4 Theoretical Perspective

Since Newton's second law of motion introduced by Sir Isaac Newton in 1686, studies on fluid has been developed rapidly. This was shown by the findings of Euler's Equation, which applied for both compressible and incompressible flow, to explain the fluid motion governing adiabatic and inviscid flow derived from Newton's second law in 1757.

Almost one century thereafter, Navier, Poisson, Saint-Venant, and Stokes developed his equation in fluid motion by introducing the effect of element of viscosity between 1827 and 1845. The Equation is called Navier-Stokes Equation and is only valid for incompressible flow. At the beginning of the 20th century, Orr-Sommerfeld Equation has derived by William McFadden Orr and Arnold Sommerfeld to describe the linear 2D modes of disturbance to a viscous parallel flow, which will be used later on the thesis, by linearizing the Navier-Stokes Equation.

This addition of viscosity produces the boundary layer which acts to the surface of a body. The boundary layer is an extremely thin layer of viscous fluid close to the surface of a solid body in contact with a stream in motion in which the region starts from where its velocity is less than its free stream velocity, and then decreases in a parabolic basis.

In engineering applications, the concept above has been used widely in transportation industries, aerospace industries in particular. To be more specific, the equation has been used for the development of an airfoil, which is a cross-section of an aircraft wing.

Practically, aircrafts are flying through free stream velocity, assumed to be uniform and laminar flow. Due to the natural characteristics of the airfoil, it is possible for the flow to change from laminar to turbulent flow when passing through the airfoil. It occurs in a certain region in the surface when the flow starts to separate from the surface of the body. This point is called a transition point.

Both laminar and turbulent flow are common and natural phenomena to occur in an airfoil. They even still produce drag force on each type of flow. In laminar flow, the friction of the body surface creates a friction drag. While in turbulent flow, the fluid motion is characterized by chaotic changes in pressure and flow velocity, thus it creates drag force. Nevertheless, the drag force can not be eliminated since it will always be correlated and created when producing lift force.

In view of the fact that both forces will always be generated, the solution to this case is to analyze the effect of Reynolds number and wavenumber to the stability and transition flow, through which an optimum lift to drag ratio may be achieved. The word optimal here will always refer to the fuel consumption, time of travel and flying comfort. To be more specific, the transition point affects the amount of the lift to drag ratio. Variables that could affect the transition point are surface geometry and material, angle of attack, velocity, and environment. Current development mostly focused on the geometry and material of the body surface to achieve the desired location of the transition point, hence producing the appropriate lift to drag ratio as well.

## 1.5 Research Scope and Limitation

The research scopes and limitations for this study are:

1. The base flow is incompressible suction boundary layer flow.
2. No heat transfer in and out of boundary layer.
3. Momentum due to gravitational force is neglected.
4. Small perturbation in the transverse direction is included in the governing equation.
5. Perturbation in streamwise and spanwise directions are neglected.
6. The transverse momentum is completely damped by the viscosity on the boundary layer.

## 1.6 Methodology

Steps that will be taken for this thesis are:

1. Apply the Orr-Sommerfeld Equation for the specific base flow.
2. Apply the equation with a spectral collocation method.
3. Arrange the equation to satisfy the generalized eigenvalue problems.
4. Develop the numerical tool by using scientific computational softwares (MATLAB and Python).
5. Execute the programmed numerical tool to calculate the eigenvalues.
6. Analyze the stability and transition of the obtained eigenvalues.
7. To confirm the results in this research, comparison with the results with other studies is considerably substantial.

## 1.7 Design and Instrumentation

This research will be done by a spectral collocation method. Consequently, a scientific computational tool, which is Python, will be assigned. After the equation has been derived, a program through the software will be made to calculate the transition point.

Various constraints that affect the determination of the transition point will also be applied in order to acquire more accurate results. Two variables, namely Reynolds number and wavenumber, will be varied for case studies. Its influence to the boundary layer will substantially be taken into account.

## 1.8 Data Analysis

The data analysis for this research will be conducted by using a numerical method. By varying the Reynolds number and wavenumber, the eigenvalues (output) will be used to examine the transition flow, stability and disturbance growth.

## CHAPTER 2

### LITERATURE REVIEW

#### 2.1 Introduction to Boundary Layer

A concept that ultimately transformed the viscous flows analysis in the twentieth century and with which the empirical experiment of drag and flow separation over a surface were feasible, is called a boundary layer. Ludwig Prandtl, a German Engineer who first introduced this theory in 1904, stated that when a freestream fluid moves through an aerodynamic body, the flow will be divided into two layers (Abidin, 2015), as illustrated in Figure 2.1.

- **Inner layer**

Inside this thin layer where  $0 \leq y \leq \delta$ , the effect of viscous force is of importance. This layer is the so-called a boundary layer. Deceleration of fluid velocity has occurred in this zone in view of the fact that it is a non-slip condition at the boundary surface. This retarded layer leads to further deceleration for the adjacent layer. Thus, generating a thin layer in which the flow velocity increases from zero at the solid surface to the value approaches the velocity of the freestream velocity.

The existence of velocity gradient inside this boundary layer region affects the fluid particle to twist seeing that the upper part of the particle has a larger speed than its bottom. Consequently, this fluid layer can be assumed as a *rotational flow*.

- **Outer layer**

On this outer flow region where  $y \geq \delta$ , the viscous force is quite inadequate and can be neglected. The absence of the velocity gradient in this layer causes

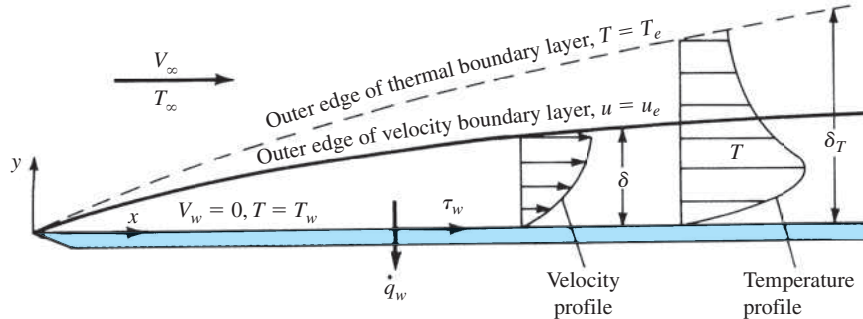


FIGURE 2.1: Properties of boundary layer (Anderson, 2016)

the fluid particle will not rotate as soon as it enters the outer flow region. Hence, the flow can be assumed as an *irrotational flow*.

Prandtl's concept of a boundary layer adjacent to an aerodynamic body results in the reduction and simplification of Navier-Stokes equations to a more amenable form by neglecting certain terms called the *boundary-layer equations*. Successively, these boundary-layer equations can be solved to achieve the distributions of shear stress and aerodynamics heat transfer to the surface.

### 2.1.1 Boundary Layer Properties

Consider a viscous flow over a flat surface with a certain length in the  $x$  direction as depicted in Figure 2.1 from (Anderson, 2016). The  $y$  – axis indicates the vertical distance from the flat plate surface. The viscous effects are included inside the thin layer adjacent to the surface. For clarity, the thickness of the layer is overemphasized.

#### Boundary-Layer Thicknesses

The no-slip condition allows the flow velocity at the surface to be zero. The flow velocity increases to the value of freestream velocity  $U_\infty$  above the surface up to a distance equal to  $\delta$ . To enhance the accuracy,  $\delta$  is determined to be the *velocity boundary-layer thickness*, which is the height over the surface with  $u = 0.99u_e$ . The velocity at the outward side of the boundary layer denoted by  $u_e$ . For this reason,

$u_e = V_\infty$ . The change in  $u$  at  $0 \leq y \leq \delta$ , that is  $u = u(y)$ , is defined as the *velocity profile* at the boundary layer at a given  $x$  point. For each of the  $x$  station, the velocity profile is different as well.

Correspondingly, the fluid temperature at the surface, which is called the *wall temperature*  $T_w$ , is equal to the surface temperature. The flow temperature varies above the surface, ranging from  $T_w \leq T \leq T_e$  at  $0 \leq y \leq \delta_T$ .  $\delta_T$  denotes as the *thermal boundary-layer thickness*. The variation of  $T$ , that is  $T = T(y)$ , is called the *temperature profile* within the boundary layer at any given  $x$  station. Since the temperature at the outer edge of the boundary layer is  $T_\infty$ , then  $T_e = T_\infty$ .

From here, two boundary layers can be concluded as a velocity boundary layer with thickness  $\delta$  and a temperature boundary layer with thickness  $\delta_T$ . In broad terms,  $\delta \neq \delta_T$  since the Prandtl number affects the relative thicknesses. If  $Pr = 1$ , then  $\delta = \delta_T$ ; if  $Pr > 1$ , then  $\delta_T < \delta$ ; if  $Pr < 1$ , then  $\delta_T > \delta$ . As evidenced in Figure 2.1, the thermal boundary layer has a larger thickness than the velocity boundary layer as  $Pr = 0.71$  for air at standard condition. It should be noticed that both boundary layer thicknesses improve with the distance  $x$  from the leading edge, which is  $\delta = \delta(x)$  and  $\delta_T = \delta_T(x)$ .

### Shear Stress And Heat Transfer

The velocity gradient at the surface induces the development of shear stress at the surface,

$$\tau_w = \mu \left( \frac{\partial u}{\partial y} \right)_w \quad (2.1)$$

where  $(\partial u / \partial y)_w$  is the velocity gradient calculated at  $y = 0$  (i.e. at the surface). Correspondingly, heat transfer at the surface is generated by the temperature gradient at the surface,

$$\dot{q}_w = -k \left( \frac{\partial T}{\partial y} \right)_w \quad (2.2)$$

where  $(\partial T / \partial y)_w$  is the temperature gradient calculated at  $y = 0$  (i.e. at the surface). It should be remarked that  $\tau_w$  and  $\dot{q}_w$  are functions of distance  $x$  from the leading edge, which is  $\tau_w = \tau_w(x)$  and  $\dot{q}_w = \dot{q}_w(x)$ .

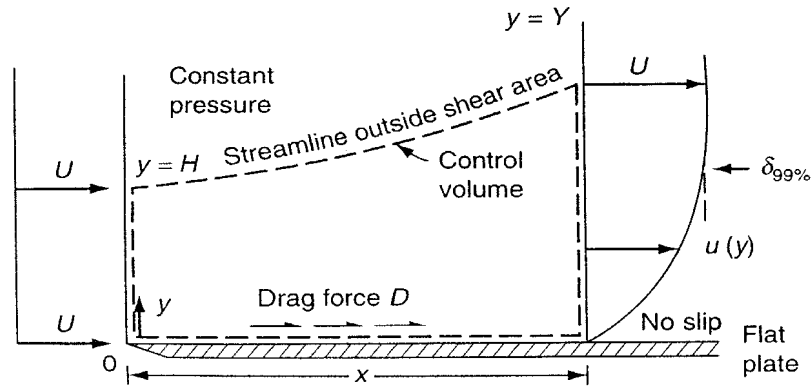


FIGURE 2.2: Control volume definition for the analysis of flow through a flat plate (White, 2006)

### Displacement Thickness

Consider a flow of fluid past through a stationary aerodynamic surface with velocity  $U$  as exemplified in Figure 2.2. In the region of boundary layer, the velocity gradient is generated with the appearance of viscosity and no-slip condition at the surface. For this control volume, conservation of mass is acquired by assuming a steady and incompressible flow. Notice that  $Y = H + \delta^*$ , the mass-flow rate can be stated as follows (White, 2006):

$$\delta^* = \int_0^{Y \rightarrow \infty} \left(1 - \frac{u}{U}\right) \quad (2.3)$$

Equation 2.3 conveys the proper definition of the *boundary-layer displacement thickness*  $\delta^*$  (function of  $x$ ) to determine conservation of mass in steady flow, as illustrated in Figure 2.3. It represents the streamlines displacement at the outer flow generated by the boundary layer. It applies for any incompressible flow, both laminar and turbulent, constant or variable temperature, and constant or variable pressure.

### 2.1.2 Laminar and Turbulent Boundary Layer

The boundary layer is either laminar or turbulent. The flow is completely *laminar* near the leading edge in which each level shifts past the nearby layers. In addition to

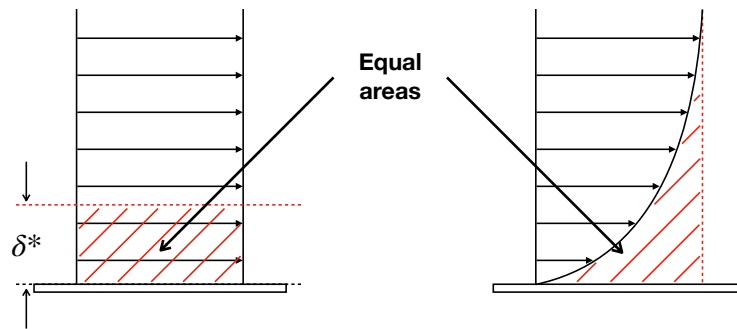


FIGURE 2.3: Displacement thickness of boundary layer

that, any interchange of mass or momentum of fluid particles occurs only between adjacent layers and is not mixed, as illustrated in Figure 2.4. Subsequently, the shear stress within the fluid is utterly a function of the viscosity  $\mu$  and velocity gradients. The speed of flow within each layer is constant and increase with the distance  $y$  from the wall. The laminar boundary layer is generated within a range of small Reynolds numbers.

On the contrary, the turbulent flow turns out to be unstable and particles of fluid tends to move both perpendicular and parallel to the wall. Ergo, the previously homogeneous flow begins to converge and fluid particles are transferred across the neighboring surfaces, as shown in Figure 2.4. This kind of flow is known as *turbulent* as a result of this apparently random movement.

Compared to the laminar boundary layer, the change of mass, energy and momentum is on a significantly higher rate. Owing to the greater extent of mixing in the main flow, the boundary layer thickness  $\delta$  increases at a quicker rate in a turbulent boundary layer. Nevertheless, in the immediate proximity of the wall, the random irregularities and mixing in turbulent cannot appear. From Figure 2.5, a viscous sublayer forms underneath the turbulent boundary layer in which the flow is laminar (*On Boundary Layers: Laminar, Turbulent and Skin Friction*, 2016; *Laminar and Turbulent Boundary Layers*, 2005).

In this thesis however, further explanation on turbulent boundary layer is refrained from discussion since the main topic is laminar boundary layer.

A STUDY OF LAMINAR-TURBULENT TRANSITION ON TWO-DIMENSIONAL SUCTION BOUNDARY LAYER

---

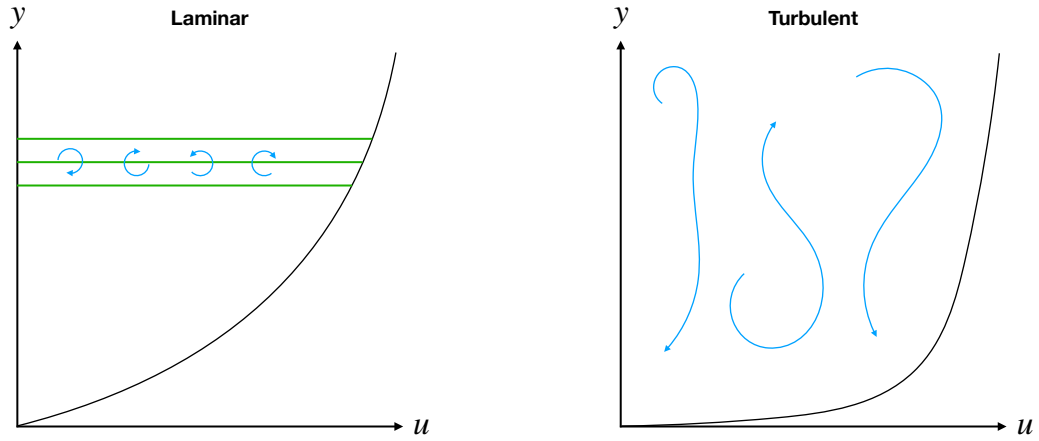


FIGURE 2.4: Common velocity profiles for laminar and turbulent boundary layers

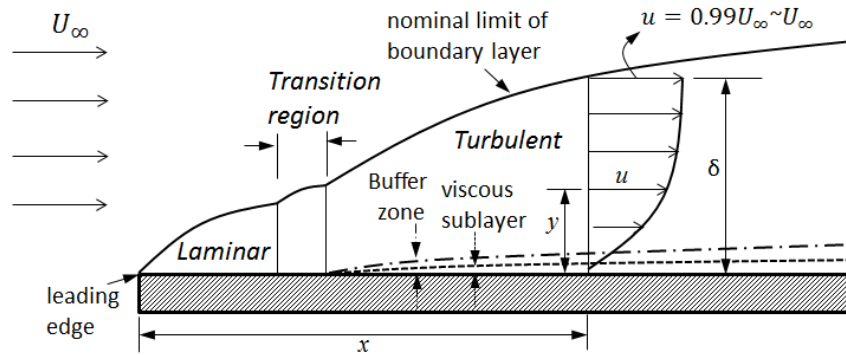


FIGURE 2.5: Phase of transition from laminar to turbulent boundary layer (Shahmohamadi & Rashidi, 2017)

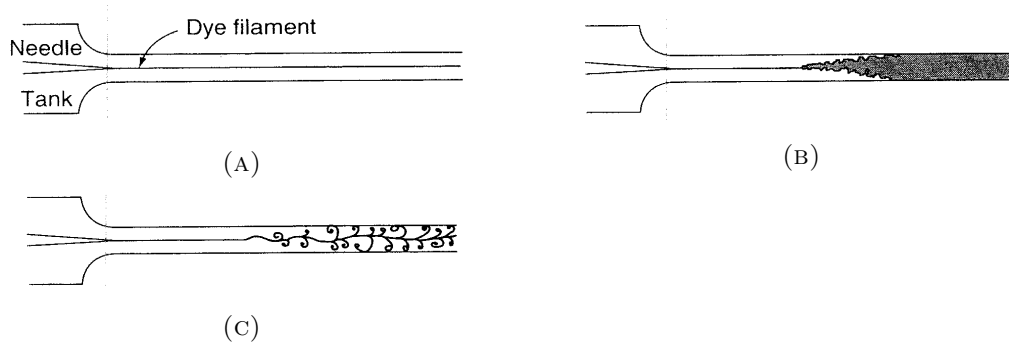


FIGURE 2.6: The classic pipe-flow dye experiment of (Reynolds, 1883): (a) low speed: laminar flow; (b) high speed: turbulent flow; (c) spark photograph of condition (b)

## 2.2 Laminar to Turbulent Transition of Boundary Layer

The linearized stability theory predicts the extermination of laminar flow specific certain Reynolds number. Turbulence is known as the early disruption of laminar flow by way of enlargement of miniscule disturbances, the flow streams through a complex order of spatial alterations, which leads to capricious and random yet oddly reasonable and wondrously stable occurrence. Transition is then defined as the entire shifting process from laminar to turbulent flow (White, 2006).

As shown in Figure 2.6, a transition experiment in a pipe flow by inserting dye into the inlet of a spherical duct was conducted (Reynolds, 1883). As can be seen in Figure 2.6a, the flow remained laminar at low speed  $Re < 2000$ , and the dye remained along a closely straight and distinct streamline. When the speed was given a rise to a range of  $Re$  between 2000 and 13000, the streamline separated somewhere downward and combined expeditiously with the surrounding water in the pipe, as shown in Figure 2.6b. A spark photograph in Figure 2.6c exposes that the instantaneous filament is still restrained to a different set of curls and eddies.

### 2.2.1 The Transition Process

The process of transition in boundary-layer flow through a soft wall comprises of the processes as follows (White, 2006):

1. Laminar flow around the leading edge in a stable state.
2. Two-dimensional Tollmien-Schlichting waves begin to be unstable.
3. Generation of hairpin eddies and three-dimensional unstable waves.
4. Vortex separation at areas of major localized shear.
5. Cascading vortex distribution into completely three-dimensional fluctuations.
6. Creation of turbulent locations at locally strong fluctuations.
7. Unification of spots into completely turbulent flow.

### 2.2.2 Classification of Transition Process

In fluids engineering, there are several mechanisms of transition process in boundary layer. The modes of transition are:

1. *Natural transition*

This is the step-by-step process of Figure 2.7 and 2.8 due to infinitesimal disturbances which has already described in the explanation above. This transition is the most common appearance mechanism on transport aircraft during a flight (Medida, 2014).

2. *Bypass transition*

The initial phases of natural instability may be missed by the flow if the surfaces vibrating or are rough, the freestream moves disorderly, or the flow subjected to acoustic waves. Thus, it will pass immediately to vortex breakdown or turbulent spots generation. This bypass is caused by large disturbances.

3. *Separated-flow transition*

"When a laminar boundary layer separates, transition may occur in the shear layer of the separated flow as a result of the inviscid instability mechanism (Langtry et al., 2006)". Some examples which cause the separation are adverse pressure gradient, trip wires, and airfoil leading edge which has a small radius (Islam, 2015).

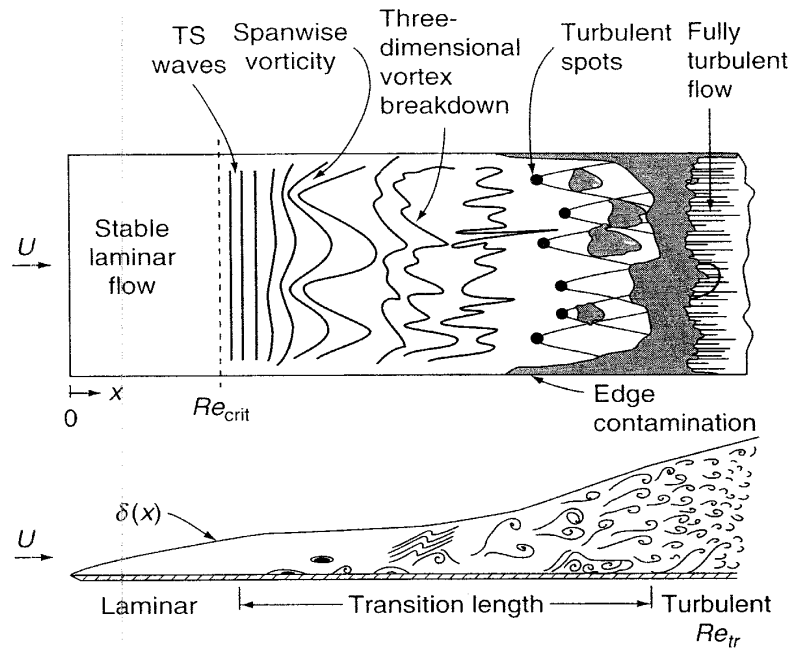


FIGURE 2.7: Idealized sketch of flat-plate flow boundary-layer transition process (Courtesy of J. T. Keegelman and T. J. Mueller, University of Notre Dame)

#### 4. Wake Induced Transition

The most significant impact of instability on transition is due to the periodic crossing of wakes from upstream leading edge and is known as "wake-induced" transition (Mayle, 1991). "One very important instance of bypass transition arises in turbomachinery flows where the blade rows are subjected to periodically passing turbulent wakes (Langtry et al., 2006)".

#### 5. Reversed Transition

This category is also referred to *relaminarization*. If the flow is greatly speeded up, this transition from turbulent to laminar flow is highly feasible (Langtry et al., 2006). An equilibrium between convection, production, and dissipation of turbulent kinetic energy is included in this transition within the boundary layer.

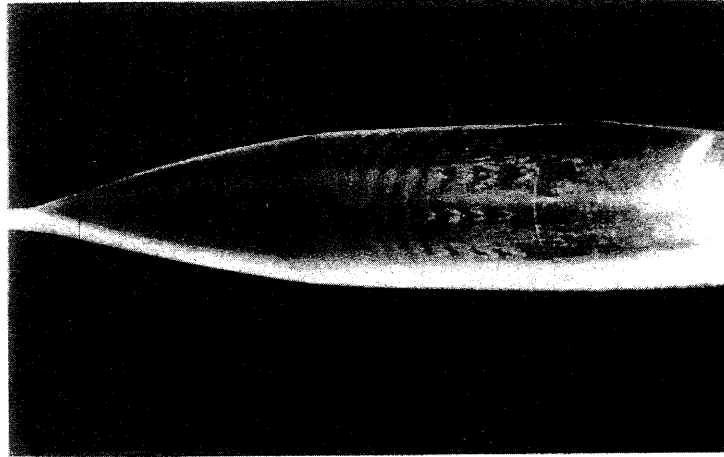


FIGURE 2.8: Smoke-flow visualization of flow with transition induced early by acoustic input at  $Re_L = 814,000$  and  $500Hz$ . (*Courtesy of J. T. Kegelmann and T. J. Mueller, University of Notre Dame*)

### 2.2.3 Important Parameters that Affect Laminar to Turbulent Transition

The basic theory of transition has never been prevailed, but a number of parameters based on experiments are conceivable to forecast the final appearance of totally turbulent stream. Comprehensibly, only one or two of the parameters are being addressed in most of the estimation. The parameters are as follows:

1. Freestream turbulence;
2. Wall roughness;
3. Pressure gradient;
4. Wall suction or blowing;
5. Wall heating or cooling.

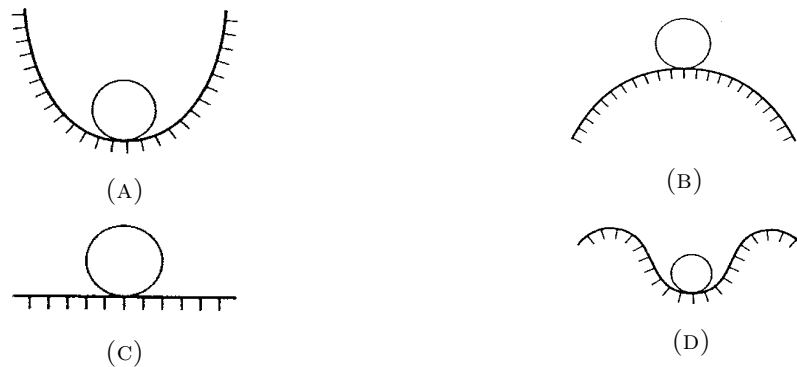


FIGURE 2.9: Relative stability of a ball at rest (White, 2006): (a) stable; (b) unstable; (c) neutral stability; (d) stable for small disturbances but unstable for large ones

## 2.3 Theory of Stability

As briefly discussed in Chapter 1, the laminar to turbulent transition can be predicted from theory of stability. Laminar flows have a serious imperfection on its poor resistancy to high Reynolds numbers. There is a certain Reynolds number which jeopardize its very presence for any given laminar flow. Higher Reynolds numbers tends to make the flow always turbulent, i.e., randomly unstable, disorderly, mostly impracticable to be analyzed accurately, yet favorably compliant to examine of its average values.

Coffee stirred in a mug mixes turbulently. Water flow through a bathroom shower duct passes turbulently. Smoke rises from a chimney rises in turbulent. Moreover, the boundary layer on a wing of commercial aircraft streams turbulently. Concurrently, laminar flow should still be taken into account since many pragmatic events appear that are laminar, namely low-speed flows, small-scale bodies, high-viscosity fluids, or leading-edge concerns.

The basic concept of stability has been addressed frequently and loquaciously by Cunningham (1963). This question will often be confined to the discussion: Can a certain physical state withstand a disturbance and likely to return to its original state? If so, then it is *stable*. If not, that is what we called the *unstable* state (White, 2006).

### 2.3.1 The General Concept of Stability

Figure 2.9 is a simple instance to explain the concept of stability, where a ball stands at rest under multiple conditions. In Figure 2.9a, the position of the ball is unconditionally stable as it would yield to its originating position even if a huge disturbance is applied. As opposed to that, an unstable state is shown in Figure 2.9b owing to the fact that the ball would fall and never to return by any trivial disturbance. Figure 2.9c is a case of neutral stability because the ball will rest on its flat surface anywhere it is displaced. Lastly, Figure 2.9d shows a more complicated situation in which the ball is stable for minor travels yet will deviate if disturbed quite a distance to topple over the side limit.

The above case is frequently occurred in the flow of boundary-layer, where a cable can affect an otherwise stable laminar flow transformed into turbulent. It should be pointed out that stability needs only a yes or no answer. We can confirm that laminar flow in viscous flow is unstable after it reaches particular Reynolds numbers. Since turbulence is an experimental basis fact, the analysis does not predict turbulence. It has never been demonstrated mathematically that turbulent flow is the adequate stable state at elevated Reynolds numbers. For that reason, we can only address the *transition* in a qualitative approach. It is determined as the alteration, over space and time and a particular Reynolds number range, of a laminar flow into a turbulent flow (White, 2006).

### 2.3.2 Inviscid-Stability Theory

In the case of an infinite Reynolds number, in which the viscosity is negligible, we can also cancel out the term of  $\nu$  in the Orr-Sommerfeld equation in Eq. 2.36. From this, we can get the relation of an inviscid-disturbance

$$\phi'' - \left( \frac{U''}{U - c} + \alpha^2 \right) \phi = 0 \quad (2.4)$$

which is named after Lord Rayleigh. The equation can be solved either analytically or numerically. The equation also asserts a point of inflection to be an origin of possible instability as Reynolds number advances infinity. Conditions on the tangential velocity  $u$  can not be maintained since the Rayleigh equation is second

order. On the boundary layer, the condition is

$$\phi(0) = \phi(\infty) = 0 \quad (2.5)$$

### 2.3.3 Viscous-Stability Theory

All kinds of laminar profiles turns out to be unstable at certain Reynolds numbers. These unsteadiness are indicated in the eigenvalues of the Orr-Sommerfeld equation which will be discussed more detailed in further section. The dimensionless final form is:

$$(\bar{U} - \bar{c}) (\bar{\phi}'' - \alpha_\delta^2 \bar{\phi}) - \bar{U}'' \bar{\phi} + \frac{i}{\alpha_\delta Re_\delta} (\bar{\phi}'''' - 2\alpha_\delta^2 \bar{\phi}'' + \alpha_\delta^4 \bar{\phi}) = 0 \quad (2.6)$$

The boundary layer conditions for this relation are

$$\begin{aligned} \phi(0) &= \phi'(0) = 0 \\ \phi(\infty) &= \phi'(\infty) = 0 \end{aligned} \quad (2.7)$$

The eigenvalues  $\alpha_\delta$  and  $\bar{c}$  can be determined with a specified velocity profile  $U(y)$  and varying  $Re_\delta$ . The situation can be evaluated for either temporal stability (real  $\alpha_\delta$ ) or spatial stability (real  $\bar{\omega} = \alpha_\delta \bar{c}$ ). The result will be unstable if we find eigenvalues for temporal instability

$$\bar{c}_i > 0 \quad (2.8)$$

and spatial instability

$$\alpha_{\delta_i} < 0 \quad (2.9)$$

To satisfy the freestream boundary conditions in Eq. 2.7, we set  $\bar{U}'' = 0$ .

The theories of viscosity forecast a limited area at low Reynolds numbers (of the order of  $Re_\delta$ ) where infinitesimal disturbances are magnified ( $c_i$  greater than zero). The boundary of this region is what we called the *neutral curve* ( $c_i = 0$ ). As shown in Figure 2.10, Two examples of a *thumb curves* are sketched. Entire disturbances are damped outside the thumb. The thumb diminishes at a large

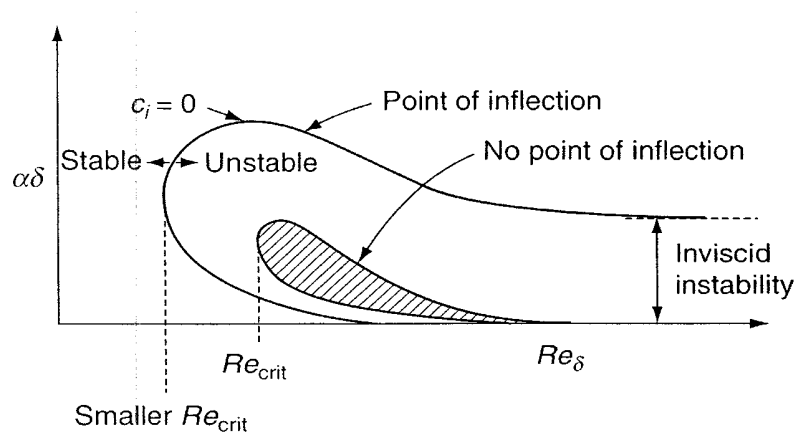


FIGURE 2.10: Neutral curves of the Orr-Sommerfeld equation  
 (White, 2006)

Reynolds number if the profile  $U(y)$  has no point of inflection. On the other hand, the thumb curve keeps open at infinity if the profile  $U(y)$  has a point of inflection.

$Re_{crit}$ , at which the disturbances can be magnified, is the lowest Reynolds number to which the thumb excels. Normally, the profile of inflection has a lower  $Re_{crit}$  and a larger thumb curve. The point of transition to turbulence intervenes at about 10 to 20 times the distance  $x_{crit}$  further downstream in the boundary layer.

## 2.4 Governing Equations

### 2.4.1 Navier-Stokes Equation

The development of mathematical models began at the last of the 19<sup>th</sup> century after the industrial revolution, despite the fact that fluid movement is an exploratory subject. In the published article "Principia" by Sir Isaac Newton (1687), in which dynamic action of fluids within invariable viscosity was studied, the original proper definition of the viscous fluid motion was suggested (White, 2006).

Subsequently, Daniel Bernoulli (1738) and Leonhard Euler (1755) formulated the inviscid stream formula, which is known as the Euler's inviscid equations. While Claude-Louis Navier (1827), Augustin-Louis Cauchy (1828), Siméon Denis Poisson (1829) and Adhémar St. Venant (1843) had examined the mathematical model

of fluid flow, the viscous (frictional) force had ignored however. In 1845, by introducing Newtonian viscous terminology, Sir George Stokes had developed the equation of motion for a viscosity-based stream, therefore taking the Navier-Stokes equations to their final form, which has since been used to produce mathematical solutions of fluid flow (White, 2006; Stokes, 1851).

Cases of thermofluid driven by regulating formulas are based on the conservation laws. The Navier-Stokes equations are the widely used mathematical model to evaluate alterations during dynamic and/or thermal interactions on these properties. The equations are adjustable in terms of the case's context and are demonstrated on the basis of the principles of mass, momentum and energy conservation (White, 2006):

- Conservation of **Mass**: *Continuity Equation*
- Conservation of **Momentum**: *Momentum Equation of Newton's Second Law*
- Conservation of **Energy**: *First Law of Thermodynamics or Energy Equation*

### 2.4.2 Conservation of Mass

In compliance with physical laws, the mass in the control volume can neither be created nor destroyed. Conservation of mass, commonly known as the Continuity Equation, notes that the variation in flow of mass between the inlet and outlet portion is zero throughout the cycle (*What are the Navier-Stokes Equations?*, n.d.):

$$\frac{D\rho}{Dt} + \rho (\nabla \cdot \vec{V}) = 0 \quad (2.10)$$

where  $\rho$  is density,  $V$  is the velocity and gradient operator  $\nabla$ . The flow is assumed to be incompressible flow. Hence, the Continuity Equation is simplified as below:

$$\frac{\partial u}{\partial x} + \frac{\partial v}{\partial y} + \frac{\partial w}{\partial z} = 0 \quad (2.11)$$

### 2.4.3 Conservation of Momentum

This relation describes the Newton's Second Law of Motion in fluid motion (incompressible flow) which utters a balance between applied force and the resulting

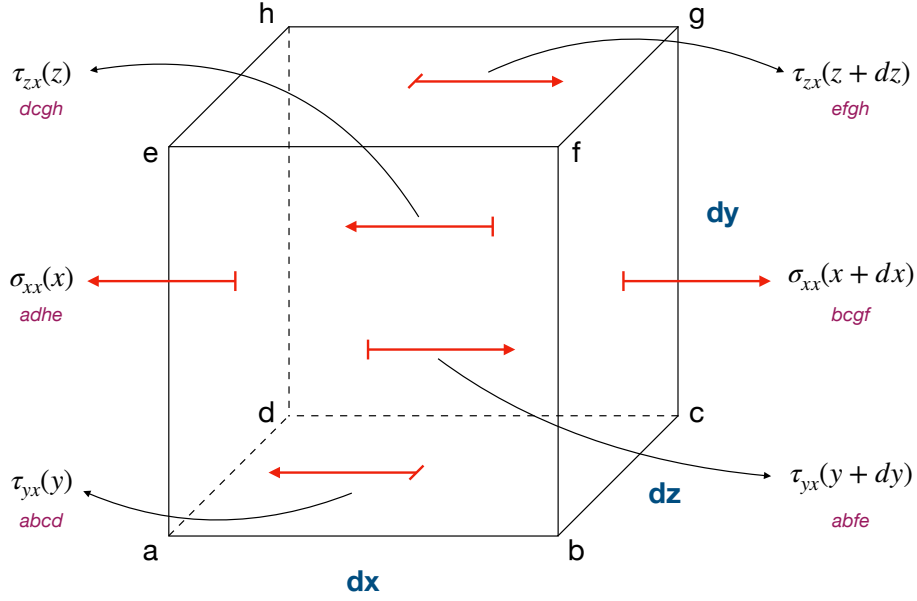


FIGURE 2.11: Notation for stresses in  $x$  component

acceleration of a particle of mass  $m$ :

$$F = ma \quad (2.12)$$

In order to make the explanation easier to be understood, we will only analyze all the total forces acting on the  $x$  component of an infinitesimally fluid, as depicted in Figure 2.11.

The total forces acting on the  $x$  component are caused by gravity

$$f_{body} = mg_x \quad (2.13)$$

$$= \rho dx dy dz g_x \quad (2.14)$$

as well as pressure and viscosity

$$\begin{aligned} f_{surface} = & \tau_{xx}(x+dx)dydz - \tau_{xx}(x)dydz + \tau_{yx}(y+dy)dx dz \\ & - \tau_{yx}(y)dx dz + \tau_{zx}(z+dz)dx dy + \tau_{zx}(z)dx dy \end{aligned} \quad (2.15)$$

The right hand side of the Newton's equation will be

$$ma_x = \rho dx dy dz a_x \quad (2.16)$$

where

$$a_x = \frac{du}{dt} \quad (2.17)$$

Since  $u$  is the function of  $x$ ,  $y$ ,  $z$ , and  $t$ , chain rules should be applied.

$$a_x = \frac{\partial u}{\partial t} + \frac{\partial u}{\partial x} \frac{dx}{dt} + \frac{\partial u}{\partial y} \frac{dy}{dt} + \frac{\partial u}{\partial z} \frac{dz}{dt} \quad (2.18)$$

where  $dx/dt = u$ ,  $dy/dt = v$ , and  $dz/dt = w$ . Then,

$$a_x = \frac{\partial u}{\partial t} + u \frac{\partial u}{\partial x} + v \frac{\partial u}{\partial y} + w \frac{\partial u}{\partial z} \quad (2.19)$$

Gathering all the known variables, relating the normal stress with the shear stress, and performing some rearrangements, the Navier-Stokes equation becomes

$$\rho g_x - \frac{\partial p}{\partial x} + \mu \frac{\partial^2 u}{\partial x^2} + \mu \frac{\partial^2 u}{\partial y^2} + \mu \frac{\partial^2 u}{\partial z^2} = \rho \left( \frac{\partial u}{\partial t} + u \frac{\partial u}{\partial x} + v \frac{\partial u}{\partial y} + w \frac{\partial u}{\partial z} \right) \quad (2.20)$$

which consists of pressure gradient, shear friction, and momentum.

#### 2.4.4 Orr-Sommerfeld Equation

For fluid dynamics, the formula Orr-Sommerfeld is an equation of eigenvalue that defines the linear two-dimensional disruption modes to a viscous parallel stream. The solution to the Navier-Stokes equation for a parallel, laminar flow can increase the growth of instability if some circumstances on the flow are met, and the Orr-Sommerfeld equation determines exactly what the situations for hydrodynamic stability are. The formula was modeled after William McFadden Orr and Arnold Sommerfeld who improved it at the beginning of the 20<sup>th</sup> century.

Starting from the method of small disturbances, the base flow can be assumed as

$$\begin{aligned} U &= U(y) \\ V &= 0 \\ W &= 0 \end{aligned} \tag{2.21}$$

and the fluctuation flow as follows:

$$\begin{aligned} u^f &= u^f(x, y, t), \quad v^f = v^f(x, y, t) \\ u &= U + u^f, \quad v = V + v^f, \quad w = 0, \quad p = P + p^f \end{aligned} \tag{2.22}$$

From the Navier-Stokes equations, we apply the continuity equation

$$\frac{\partial u}{\partial x} + \frac{\partial v}{\partial y} + \frac{\partial w}{\partial z} = 0 \tag{2.23}$$

and momentum equation:

x-momentum

$$\frac{\partial u}{\partial t} + u \frac{\partial u}{\partial x} + v \frac{\partial u}{\partial y} = -\frac{1}{\rho} \frac{\partial P}{\partial x} + \nu \left[ \frac{\partial^2 u}{\partial x^2} + \frac{\partial^2 u}{\partial y^2} \right] \tag{2.24}$$

y-momentum

$$\frac{\partial v}{\partial t} + u \frac{\partial v}{\partial x} + v \frac{\partial v}{\partial y} = -\frac{1}{\rho} \frac{\partial P}{\partial y} + \nu \left[ \frac{\partial^2 v}{\partial x^2} + \frac{\partial^2 v}{\partial y^2} \right] \tag{2.25}$$

Substituting Eq. 2.21 and 2.22 into Eq. 2.23

$$\begin{aligned} \frac{\partial(U + u^f)}{\partial x} + \frac{\partial(V + v^f)}{\partial y} &= 0 \\ \frac{\partial U}{\partial x} + \frac{\partial V}{\partial y} + \frac{\partial u^f}{\partial x} + \frac{\partial v^f}{\partial y} &= 0 \end{aligned} \tag{2.26}$$

Since  $(\partial U/\partial x) + (\partial V/\partial y) = 0$ , then

$$\frac{\partial u^f}{\partial x} + \frac{\partial v^f}{\partial y} = 0 \tag{2.27}$$

By applying base and fluctuating flow, substituting Eq. 2.21 and 2.22 into Eq. 2.24 we derive

$$\begin{aligned}
 & \frac{\partial(U + u^f)}{\partial t} + (U + u^f) \frac{\partial(U + u^f)}{\partial x} + (V + v^f) \frac{\partial(U + u^f)}{\partial y} = \\
 & \quad - \frac{1}{\rho} \frac{\partial(P + p^f)}{\partial x} + \nu \left\{ \frac{\partial^2(U + u^f)}{\partial x^2} + \frac{\partial^2(U + u^f)}{\partial y^2} \right\} \cdot \\
 & \quad \quad \quad \left[ \frac{\partial U}{\partial t} + U \frac{\partial U}{\partial x} + V \frac{\partial U}{\partial y} \right] + \quad (2.28) \\
 & \left[ \frac{\partial u^f}{\partial t} + u^f \frac{\partial U}{\partial x} + U \frac{\partial u^f}{\partial x} + u^f \frac{\partial u^f}{\partial x} + V \frac{\partial u^f}{\partial y} + v^f \frac{\partial U}{\partial y} + v^f \frac{\partial u^f}{\partial y} \right] = \\
 & \left[ - \frac{1}{\rho} \frac{\partial P}{\partial x} + \nu \left\{ \frac{\partial^2 U}{\partial x^2} + \frac{\partial^2 U}{\partial y^2} \right\} \right] + \left[ - \frac{1}{\rho} \frac{\partial p^f}{\partial x} + \nu \left\{ \frac{\partial^2 u^f}{\partial x^2} + \frac{\partial^2 u^f}{\partial y^2} \right\} \right].
 \end{aligned}$$

Since  $(\partial U / \partial x) \ll (\partial U / \partial y)$ , from base flow the  $V = 0$ , and by neglecting product of the fluctuating terms, the fluctuation x-momentum equation hence:

$$\begin{aligned}
 & \frac{\partial u^f}{\partial t} + u^f \frac{\partial U}{\partial x} + U \frac{\partial u^f}{\partial x} + u^f \frac{\partial u^f}{\partial x} + V \frac{\partial u^f}{\partial y} + v^f \frac{\partial U}{\partial y} + v^f \frac{\partial u^f}{\partial y} = \\
 & \quad - \frac{1}{\rho} \frac{\partial p^f}{\partial x} + \nu \left\{ \frac{\partial^2 u^f}{\partial x^2} + \frac{\partial^2 u^f}{\partial y^2} \right\}. \quad (2.29) \\
 & \frac{\partial u^f}{\partial t} + U \frac{\partial u^f}{\partial x} + v^f \frac{\partial U}{\partial y} + \frac{1}{\rho} \frac{\partial p^f}{\partial x} = \nu \left[ \frac{\partial^2 u^f}{\partial x^2} + \frac{\partial^2 u^f}{\partial y^2} \right].
 \end{aligned}$$

Applying the same method for y-momentum, substituting Eq. 2.21 and 2.22 into Eq. 2.25 we get

$$\begin{aligned}
 & \frac{\partial(V + v^f)}{\partial t} + (U + u^f) \frac{\partial(V + v^f)}{\partial x} + (V + v^f) \frac{\partial(V + v^f)}{\partial y} = \\
 & \quad - \frac{1}{\rho} \frac{\partial(P + p^f)}{\partial y} + \nu \left\{ \frac{\partial^2(V + v^f)}{\partial x^2} + \frac{\partial^2(V + v^f)}{\partial y^2} \right\} \cdot \\
 & \quad \quad \quad \left[ \frac{\partial V}{\partial t} + U \frac{\partial V}{\partial x} + V \frac{\partial V}{\partial y} \right] + \quad (2.30) \\
 & \left[ \frac{\partial v^f}{\partial t} + u^f \frac{\partial V}{\partial x} + U \frac{\partial v^f}{\partial x} + u^f \frac{\partial v^f}{\partial x} + V \frac{\partial v^f}{\partial y} + v^f \frac{\partial V}{\partial y} + v^f \frac{\partial v^f}{\partial y} \right] = \\
 & \left[ - \frac{1}{\rho} \frac{\partial P}{\partial y} + \nu \left\{ \frac{\partial^2 V}{\partial x^2} + \frac{\partial^2 V}{\partial y^2} \right\} \right] + \left[ - \frac{1}{\rho} \frac{\partial p^f}{\partial y} + \nu \left\{ \frac{\partial^2 v^f}{\partial x^2} + \frac{\partial^2 v^f}{\partial y^2} \right\} \right].
 \end{aligned}$$

From the base flow,  $V = 0$ , so  $(\partial V/\partial x) = 0$  and  $(\partial V/\partial y) = 0$ . Also, by neglecting product of the fluctuating terms the fluctuating y-momentum thus become

$$\begin{aligned} \frac{\partial v^f}{\partial t} + \cancel{u^f \frac{\partial V}{\partial x}} + U \frac{\partial v^f}{\partial x} + \cancel{u^f \frac{\partial v^f}{\partial x}} + \cancel{V \frac{\partial v^f}{\partial y}} + \cancel{v^f \frac{\partial V}{\partial y}} + \cancel{v^f \frac{\partial v^f}{\partial y}} = \\ -\frac{1}{\rho} \frac{\partial p^f}{\partial y} + \nu \left\{ \frac{\partial^2 v^f}{\partial x^2} + \frac{\partial^2 v^f}{\partial y^2} \right\}. \end{aligned} \quad (2.31)$$

$$\frac{\partial v^f}{\partial t} + U \frac{\partial v^f}{\partial x} + \frac{1}{\rho} \frac{\partial p^f}{\partial x} = \nu \left[ \frac{\partial^2 v^f}{\partial x^2} + \frac{\partial^2 v^f}{\partial y^2} \right].$$

In this method, the disturbances need to be modelled. The disturbances are consisted of a quantity of discrete partial fluctuations by taking into account several parameters as follows:

- Each of which propagating in  $x$  direction
- Perturbation is assumed to be 2D stream function
- Assuming any random 2D disturbance to be in Fourier Series expansion
- Each turbulence represents partial oscillations

By considering some parameters above, the model of the turbulence become

$$\psi(x, y, t) = \phi(y)e^{i(\alpha x - \omega t)} \quad (2.32)$$

$$= \phi(y)e^{i\alpha(x - ct)} \quad (2.33)$$

where  $c = \alpha/\omega$ . The model of the disturbance in the fluctuating flow then

$$\begin{aligned} u^f &= \frac{\partial \psi}{\partial y} = \phi'(y)e^{i(\alpha x - \omega t)} \\ v^f &= -\frac{\partial \psi}{\partial x} = -\phi(y)e^{i(\alpha x - \omega t)}(i\alpha) \end{aligned} \quad (2.34)$$

After modelling the disturbance, we can substitute Eq. 2.34 into momentum equation in Eq. 2.29 and 2.31

$$\begin{aligned}
 \phi'(y)e^{i(\alpha x - \omega t)}(-i\omega) + U\phi'e^{i(\alpha x - \omega t)}(i\alpha) + (-i\alpha)\phi e^{i(\alpha x - \omega t)}\frac{\partial U}{\partial y} + \frac{1}{\rho}\frac{\partial p^f}{\partial x} \\
 = \nu \left[ \frac{\partial^2}{\partial x^2} + \frac{\partial^2}{\partial y^2} \right] ((-i\alpha)e^{i(\alpha x - \omega t)}). \\
 (-i\alpha)\phi e^{i(\alpha x - \omega t)}(-i\omega + U(-i\alpha)\phi e^{i(\alpha x - \omega t)}(i\alpha) + \frac{1}{\rho}\frac{\partial p^f}{\partial y}) \\
 = \nu \left[ \frac{\partial^2}{\partial x^2} + \frac{\partial^2}{\partial y^2} \right] ((-i\alpha)\phi e^{i(\alpha x - \omega t)}).
 \end{aligned} \tag{2.35}$$

By rearrangements, expansions and differentiation, the final Orr-Sommerfeld equation is

$$(U - c)(\phi'' - \alpha^2\phi) - U'' + \frac{i\nu}{\alpha}[\phi'''' - 2\alpha^2\phi'' + \alpha^4\phi] = 0 \tag{2.36}$$

Using the following non-dimensional parameters

$$\begin{aligned}
 \bar{U} &= \frac{U}{U_e} \\
 \eta &= \frac{y}{\delta} \\
 \bar{\phi} &= \frac{\phi}{U_e\delta} \\
 \bar{c} &= \frac{c}{U_e} \\
 \alpha_\delta &= \alpha\delta \\
 Re_\delta &= \frac{U_e\delta}{\nu}
 \end{aligned} \tag{2.37}$$

The non-dimensionalized Orr-Sommerfeld equation become

$$(\bar{U} - \bar{c})(\bar{\phi}'' - \alpha_\delta^2\bar{\phi}) - \bar{U}''\bar{\phi} + \frac{i}{\alpha_\delta Re_\delta}(\bar{\phi}'''' - 2\alpha_\delta^2\bar{\phi}'' + \alpha_\delta^4\bar{\phi}) = 0 \tag{2.38}$$

## 2.5 Spectral Collocation Methods

Spectral collocation methods are applied to solve any kinds of ordinary and partial differential equations (ODEs and PDEs) which contained in problems of fluid

mechanics, vibrations, quantum mechanics, linear and non-linear waves, complex analysis, and other subjects. Spectral methods are one of the three major PDE numerical solution developments which in successive decades have become their own: finite difference methods (1950s), finite element methods (1960s), and spectral methods (1970s).

Some of the key ideas that govern the spectral methods are interpolation and expansion, as well as specific algorithmic developments. To achieve high accuracy in solving an ODE or PDE on a basic domain, the spectral methods are ordinarily the foremost tool if the information regarding the problem are smooth. They can provide accuracy up to ten digits where finite element or finite difference method would produce two or three digits of accuracy (Trefethen, 2000).

### 2.5.1 Smoothness and Spectral Accuracy

Methods of spectral and finite elements have a strong relationship and are based on the similar concepts. The primary difference between them is that spectral approaches utilize non-null base functions over the whole domain and non-null base functions on limited subdomains using finite element methods. Alternatively stated, spectral methods take a global approach whereas finite element methods apply a local approach (Canuto, 2007).

Partly for that basis, spectral methods have outstanding errors with a smooth solution having the so-called exponential convergence. The common convergence rate is  $\mathcal{O}(N^{-m})$  for every  $m$  for functions that are smooth and  $\mathcal{O}(c^N)$  ( $0 < c < 1$ ) for functions that are analytic. Aforementioned behavior is called *spectral accuracy*.

The Fourier transform will be utilized to obtain the relationships in an argument consisting of two measurements. First, there is a quick decaying transform in a smooth function. This is due to a smooth system that evolves gradually. Since large wave numbers equate to quickly oscillating waves, its function does not produce any energy at high numbers of waves. Furthermore, if the Fourier function conversion easily decays, then the discretionary errors are low. The reason for these errors is because high waven numbers are alienated to low waven numbers (Trefethen, 2000).

## 2.5.2 Eigenvalues and Fourth-Order Problems

Spectral methods constitute formidable tools for the calculation of eigenvalues of differential and integral operators and their generalization for highly non-symmetrical topics (pseudospectra). The calculation of critical Reynolds number  $R = 5772.22$  by Orszag (Orszag, 1971) for eigenvalue unsteadiness of plane Poiseuille flow ensured an obvious confirmation to demonstrate spectral methods to be a substantial equipment in scientific computing due to its high accuracy.

An instance of the fourth-order spectral computation is the Orr-Sommerfeld equation from the field of hydrodynamic stability. The solution of Navier-Stokes equation is a laminar flow which is comprised of a smooth horizontal movement with a parabola speed velocity when the flow is undertaken by a constant pressure gradient between two infinite flat plates at Reynolds number (non-dimensionalized velocity)  $Re$ . The solution can be obtained by applying an uncomplicated technique including polynomials related by  $p(x) = (1 - x^2)q(x)$  (Trefethen, 2000).

For  $Re \gg 1000$ , the flow is invariably turbulence. The laminar flow must be unstable for high  $Re$  in small disturbances. The problem of the eigenvalue of Orr-Sommerfeld equation arises from a linearized stability examination on the basis of a perturbation with the longitudinal framework  $e^{ix}$  and a development at level  $e^{\lambda t}$ :

$$Re^{-1}(u_{xxxx} - 2u_{xx} + u) - 2iu - i(1 - x^2)(u_{xx} - u) = \lambda(u_{xx} - u) \quad (2.39)$$

with boundary conditions  $u(\pm 1) = u_x(\pm 1) = 0$ . The values of  $R$  need to be determined so that the real part of the eigenvalues  $\lambda$  are positive to analyze instability. By discretization, the generalized  $(N - 1) \times (N - 1)$  eigenvalue problem  $Av = \lambda Bv$  is acquired, where

$$A = Re^{-1}(D_4 - 2D_2 + I) - 2iI - idia(1 - x_j^2)(D_2 - I), \quad (2.40)$$

$$B = D_2 - I. \quad (2.41)$$

The discretized version of the equation becomes a generalized eigenvalue problem:

$$A \cdot U = \lambda B \cdot U \quad (2.42)$$

The  $D_2$  is second derivative matrix  $\tilde{D}_N^2$  stating the boundary conditions  $u(\pm 1) =$

0, and the fourth derivative matrix denoted by  $D_4$  stating the clamped boundary conditions  $u(\pm 1) = u_x(\pm 1) = 0$ . The resulting eigenvalues spectrally converge to the Y form familiar to everyone involved in hydrodynamic stability. As intended, the rightmost value is almost on the imaginary axis (Trefethen, 2000).

## **CHAPTER 3**

### **RESEARCH METHODOLOGY**

#### **3.1 Introduction to the Method**

##### **3.1.1 Spectral Methods**

Partial differential equations (PDEs), ordinary differential equations (ODEs) and eigenvalue problems are typical cases that can be solved by spectral methods. These method benefits a sum of certain basis functions as the solution of the differential equation. The PDEs then are substituted by the functions which yield to a system of ODEs in the coefficients. Then, converts the eigenvalue problems for ODEs to matrix eigenvalue problems.

Spectral methods are implemented and accomplished normally by either of these three approaches, collocation, Galerkin or a Tau approach. The collocation approach selects finite-dimensional space of piecewise polynomial interpolants up to certain degree and a variety of collocation points in the domain. In the context of differential equations, these techniques are defined as spectral collocation methods.

##### **3.1.2 Eigenvalue and Generalized Eigenvalue Problems**

In this thesis, spectral collocation methods will be applied to solve ordinary differential equations (ODEs) for eigenvalue problems by arranging the equation matrices into a generalized eigenvalue problems.

In respect of eigenvalue problems, its eigenvectors reflect the directions of the data distribution or variation and the magnitude of its variation in such locations is its corresponding eigenvalues.

While for the generalized eigenvalue problems, the paths are influenced by another matrix. If the other matrix is the identity matrix, this effect will be cancelled

and we will have the eigenvalue problem taking the directions of the full distribution.

Below is the matrix form of generalized eigenvalue problems, with which we can solve the Orr-Sommerfeld equations

$$A \cdot \phi = \lambda B \cdot \phi \quad (3.1)$$

where  $A$  and  $B$  are a pair-symmetrical matrix, with  $\lambda$  and  $\phi$  are the eigenvalues and eigenvectors, respectively.

### 3.1.3 Spectral Collocation Methods of Asymptotic Suction Boundary Layer

Recall the non-dimensionalized Orr-Sommerfeld equation (Eq. 2.38) from Chapter 2

$$(\bar{U} - \bar{c}) (\bar{\phi}'' - \alpha_\delta^2 \bar{\phi}) - \bar{U}'' \bar{\phi} + \frac{i}{\alpha_\delta Re_\delta} (\bar{\phi}'''' - 2\alpha_\delta^2 \bar{\phi}'' + \alpha_\delta^4 \bar{\phi}) = 0$$

For simplicity, we may remove several notations in such a way so that the equation becomes

$$(U - c) (\phi'' - \alpha^2 \phi) - U'' \phi + \frac{i}{\alpha Re} (\phi'''' - 2\alpha^2 \phi'' + \alpha^4 \phi) = 0 \quad (3.2)$$

The general form of the *basic flow* for this thesis will be

$$u = U \left( 1 - e^{-\frac{yv}{\nu}} \right) \quad (3.3)$$

where  $v$  is a suction velocity and  $\nu$  is dynamic viscosity. In this case, the value of  $U = 1$  and  $(v/\nu) = 1$ . The basic flow then become  $u = 1 - e^{-y}$ . Thus, the second derivative of  $u$  is  $u'' = -e^{-y}$ . The  $u$  and  $u''$  will be substituted to the  $U$  and  $U''$  in the equation. After some substitutions and rearrangements, the equation turns into

$$Re^{-1} (\phi'''' - 2\alpha\phi'' + \alpha^4\phi) - e^{-y}i\alpha\phi - i\alpha(1 - e^{-y})(\phi^2 - \alpha^2\phi) = \lambda(\phi'' - \alpha^2\phi) \quad (3.4)$$

where  $\omega = \alpha c$  and  $\lambda = -i\omega$ .

The fundamental concept is to define a new function  $q(y)$  to handle the 4<sup>th</sup> order operator:

$$\phi(y) = (1 - e^{-y}) q(y) \quad (3.5)$$

Note that the new function  $q(y)$  complies the boundary conditions. Then, the 4<sup>th</sup> order operator in terms of  $q(y)$  becomes:

$$\frac{d^4\phi}{dy^4} = (1 - e^{-y}) \frac{d^4q}{dy^4} + 4e^{-y} \frac{d^3q}{dy^3} - 6e^{-y} \frac{d^2q}{dy^2} + 4e^{-y} \frac{dq}{dy} - e^{-y}q \equiv \tilde{D}_4q \quad (3.6)$$

In this method, every differential operator must be discretized at the points of collocation to form matrices  $\mathbb{D}_i$

$$\begin{aligned} \text{Diag}(1 - e^{-y}) \mathbb{D}_4 - 4e^{-y} \text{Diag}(y) \mathbb{D}_3 - 6e^{-y} \mathbb{D}_2 + 4e^{-y} \mathbb{D}_1 - e^{-y} &\equiv \tilde{D}_4 \Rightarrow \tilde{\mathbb{D}}_4 \\ \frac{d^1}{dy^1} &\equiv D_1 \Rightarrow \mathbb{D}_1 \\ \frac{d^2}{dy^2} &\equiv D_2 \Rightarrow \mathbb{D}_2 \\ \frac{d^3}{dy^3} &\equiv D_3 \Rightarrow \mathbb{D}_3 \\ \frac{d^4}{dy^4} &\equiv D_4 \Rightarrow \mathbb{D}_4 \end{aligned} \quad (3.7)$$

The notation  $\text{Diag}(1 - e^{-y})$  is a diagonal matrix with elements  $1 - e^{-y_i}$  along its diagonal.

The discretized form of the unknown  $q(y)$  at the points of collocation creates the vector  $Q$  which is referred to the discretized unknown  $\phi_i$  by:

$$Q_i = \frac{\phi_i}{(1 - e^{-y_i})} \quad (3.8)$$

so that

$$\tilde{\mathbb{D}}_4 Q = \tilde{\mathbb{D}}_4 S \phi \quad (3.9)$$

where

$$S = \text{Diag} \left( \frac{1}{1 - e^{-y_i}} \right) \quad (3.10)$$

Long story short, the discretized form of the Orr-Sommerfeld equation turns into

$$\left\{ Re^{-1} \left( \tilde{\mathbb{D}}_4 \mathbb{S} - 2\alpha^2 \mathbb{D}_2 + \mathbb{I}\alpha^4 \right) - e^{-y} i\alpha \mathbb{I} - i\alpha \text{Diag} \left( 1 - e^{-y} \right) \left( \mathbb{D}_2 - \mathbb{I}\alpha^2 \right) \right\} \phi = \lambda \left( \mathbb{D}_2 - \mathbb{I}\alpha^2 \right) \phi \quad (3.11)$$

where  $\mathbb{I}$  = Identity matrix and  $\text{Diag}$  = Diagonal matrix. With respect to the operators, the equation can be stated more compactly as

$$\begin{aligned} \mathbf{A} &= \left\{ Re^{-1} \left( \tilde{\mathbb{D}}_4 \mathbb{S} - 2\alpha^2 \mathbb{D}_2 + \mathbb{I}\alpha^4 \right) - e^{-y} i\alpha \mathbb{I} - i\alpha \text{Diag} \left( 1 - e^{-y} \right) \left( \mathbb{D}_2 - \mathbb{I}\alpha^2 \right) \right\} \\ \mathbf{B} &= \left( \mathbb{D}_2 - \mathbb{I}\alpha^2 \right) \end{aligned} \quad (3.12)$$

The discretized form of the Orr-Sommerfeld equation yields to a generalized eigenvalue problem:

$$\mathbf{A} \cdot \phi = \lambda \mathbf{B} \cdot \phi \quad (3.13)$$

where  $\lambda = -i\omega$ . Since this form is already established explicitly for the case, the next step is to solve this form by a specific package from the computing tools. The explanation is contained in the next section.

## 3.2 Computing Tools

### 3.2.1 Chebfun Codes for MATLAB

Chebfun is an open-source software with an embedded functions for numerical computing. It is a high-quality, well-tested and mature numerical library in solving differential equations using spectral method. By applying a piecewise polynomial interpolation with Chebyshev Series as its mathematical initial interest, it has vigorous techniques to handle linear and non-linear differential and integral operators. Still further, it can deal with partial differential equations with the involvement of one space and one time variable. It would be an enormous effort to re-implement chebfun from MATLAB in Python, hence MATLAB engine for Python is used.

### Regarding Chebops

On chebfuns, there is an operator which epitomizes an integral or differential operator, it is called chebop. To find the eigenvalues that we are willing to solve, `eigs` and `expm` is applicable to the operators. In this case, we will use only the `eigs`. The aforementioned syntax will be explained in the next section.

Similar to the chebfuns, chebops begin with an approximation of polynomial interpolants. It is also determined as spectral collocation methods, particularly for differential equations. In order to attain maximum feasible accuracy through double precision arithmetic, the discretizations will be selected automatically.

### 3.2.2 MATLAB and Python

It has been mentioned in the previous title section that chebfun codes is, currently, only available for MATLAB programming language. MATLAB is a multi-paradigm numerical computing environment developed exclusively by Mathworks. It is a high-level programming and very powerful for mathematical programming.

MATLAB is categorized as one of the oldest programming languages. Thus, various communities regarding the MATLAB codes have been provided and spreaded widely. MATLAB has its own concept with a whole package included, as well as the IDE. Below is the advantages and disadvantages of using MATLAB.

MATLAB advantages:

1. Availability of numerous packages with a compact script
2. Provides multiple threaded support and community
3. Packages for any types of mathematics and trading for the commercial level
4. According to its long experience, it is well tested and supported

MATLAB disadvantages:

1. A proprietary and closed-source software
2. Expensive, only people with sufficient funds to buy the license who can use it

3. It does not perform well for iterative loops
4. The capability of developing stand-alone applications is poor

On the other hand, Python is rather general-purpose programming language, with which we can develop fully functional apps or any software tools. Besides being a high-level programming, it also became the most straightforward syntax which we are able to translate easily our ideas into the codes. This free high-level programming language is being massively adapted, supported by its embedded and third party IDEs. To analyze other benefits of using Python, we should see the advantages and disadvantages of Python as well, explained as follows.

Python advantages:

1. It is a free, cross-platform and open-source software which we will get the libraries, lists, and dictionaries after we download and install it.
2. Reliable to work with other languages to connect, such as R, C++, and others.
3. Fastest iterative loops in the category of general-purpose programming languages
4. Python has a beautiful and simple programming language
5. Python is very structured through its indentation rule which leads to an ease to be followed

Python disadvantages:

1. Trading packages are still juvenile
2. Since it is still categorized as a new programming language, community is smaller compared to MATLAB
3. Packages are not compatible with each other

Based on the explanation and comparison above, we have come to a conclusion that we will use both programming language. The reasons to this are the existing

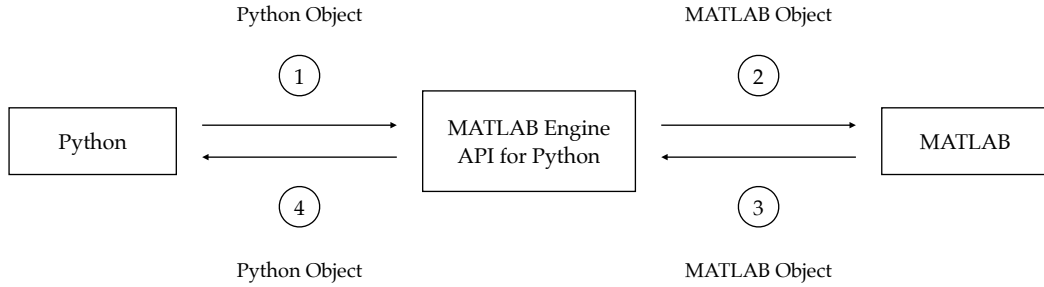


FIGURE 3.1: MATLAB Engine API for Python work process

library to solve this spectral collocation method is available in MATLAB. However, since we will perform various loops for the case then we should also use Python to perform a better calculation.

### 3.2.3 MATLAB Engine API for Python

There is a package with which Python can call MATLAB as a computational engine, it is called MATLAB Engine API for Python. The step-by-step process is illustrated in Figure 3.1. The initial step is to bring the python object from Python into the Engine API so that it can be translated into a matlab object. Now, the object is already in MATLAB programming language as a MATLAB function.

MATLAB solves the ordinary differential equations of the object with the spectral collocation method in which the function is already existed. After the equations are solved, the results and data obtained from the calculation will be transferred back to Python through Engine API to be processed and analyzed.

## 3.3 Variables

To execute the program, several variables should be considered as follows:

1. Reynolds number ( $Re$ )
  - $Re = 1 \times 10^3 - 1.5 \times 10^4$ , 150 step
  - $Re = 1.5 \times 10^4 - 1 \times 10^7$ , 985 step
  - $Re = 1 \times 10^7 - 1 \times 10^8$ , 90 step

2. Wavenumber/alpha ( $\alpha$ )

- $\alpha = 0.01 - 0.3, 0.01$  step

3. Number of eigenvalues ( $\lambda$ ), which represents the resolution of the spectral method

- $n(\lambda) = 30$

4. Boundary conditions

- $\phi(0) = \phi'(0) = 0$
- $\phi(\infty) = \phi'(\infty) = 0$

### 3.4 Prediction of Temporal Stability

To analyze this event, the disturbances have two distinct functional approaches. The numerical solution to the equation is either spatial or temporal growth of disturbances. The functional shape for temporal stability is as follows:

$$\text{Temporal growth:} \quad f(Re, \alpha, c_r, c_i) = 0 \quad (3.14a)$$

where the subscripts  $r$  and  $i$  denotes real and imaginary, respectively. In addition to the equation above, temporal growth requires real  $\alpha$  and complex  $c$ , while spatial growth should have complex  $\alpha$  and real  $\alpha c$ . If  $\lambda_{real} = 0$  for temporal growth, neutral stability is occurred. If  $\lambda_{real}$  is negative, then it is stable. But, if  $\lambda_{real}$  is positive, it is an unstable state.

In this study, temporal growth of disturbances will be discussed. A proper boundary layer conditions for the Orr-Sommerfeld equation is also considered, which is

$$\phi(0) = \phi'(0) = 0 \quad (3.15a)$$

$$\phi(\infty) = \phi'(\infty) = 0. \quad (3.15b)$$

We will be discussing about an eigenvalue problem due to the homogeneity of the equation and its corresponding boundary conditions.

## CHAPTER 4

### RESULTS AND DISCUSSIONS

#### 4.1 Computation Variables

On this study, two independent variables from the Orr-Sommerfeld Equation are being varied. As mentioned before, Reynolds number ( $Re$ ) and wavenumber ( $\alpha$ ) are the variables that affects the stability of the flow, and into some extent, the stability growth inside the boundary layer.

As mentioned in Chapter 3, Reynolds number use three variation steps to be analyzed. The first set is ranging from  $1 \times 10^3$  to  $1.5 \times 10^4$ , generating 150 points. By generating 985 points, the second set has a range of Reynolds number from  $1.5 \times 10^4$  to  $1 \times 10^7$ . The last set is ranging from  $1 \times 10^7$  to  $1 \times 10^8$  with a creation of 90 points. For the second variable, the wavenumber  $\alpha$  is linearly spaced from 0.01 to 0.3 with 0.01 step.

For the computation, the range of  $Re$  is not equally spaced; some range require high resolution some dont. Hence the computing cost can be unnecessarily high if high resolution computation is done for all range. The higher the value of  $Re$ , the more time it requires for the code to calculate at that  $Re$  value. For each  $\alpha$ , the computation takes approximately 12 hours to execute for the entire range of  $Re$ . The calculations were performed for 30 values of  $\lambda$ , hence the total computational time was  $\geq 360 h$ .

Additionally, execution time above is valid for a computer with specifications as follows:

- Operating System  
Windows 10 Pro 64-bit (10.0, Build 18362)
- Processor  
Intel(R) Core (TM) i7-6700 CPU @3.40 GHz (8 CPUs)

- Memory  
16 GB RAM
- VGA  
NVIDIA GeForce GTX 1070 8 GB

## 4.2 Data Plot for Several Wavenumbers

On this part, the results in terms of real-maximum eigenvalues ( $\lambda_{rmax}$ ) will be analyzed and discussed. The data plot of  $\lambda_{rmax}$  is achieved for wavenumber  $\alpha = 0.01 - 0.3$  with 0.01 step and Reynolds number  $Re = 1 \times 10^3 - 1 \times 10^8$  with steps as previously explained.

Each data plot will not be addressed completely one by one since, for several data plots, they are making almost the same trends. Consequently, there are only three data plots to be highlighted for discussion. Furthermore, complete plots will also be provided to have a wider observation for the entire wavenumber range.

### 4.2.1 Data Plot for Wavenumber 0.01

First plot for  $\lambda_{rmax}$  at  $\alpha = 0.01$  with an aforementioned range of  $Re$  will be discussed in this subsection, as illustrated in Figure 4.1. In general terms, this case demonstrates an exponential shifting from stable to unstable since the value of  $\lambda_{rmax}$  starts to have a positive value at about  $Re = 1.5 \times 10^7$  until the last value of  $Re$  at specified range. For some eigenvalues data for  $\alpha = 0.01$ , see appendix B.1.

The whole curve is obviously having an exponential pattern. Despite that, the first several points of  $\lambda_{rmax}$  do not satisfy the pattern. It is possible that this issue is appeared due to the mathematical model of the initial equation itself. However, this disordered  $\lambda_{rmax}$  points at the lower  $Re$  eliminate with the increasing  $\alpha$ . These chaotic points will completely vanished at  $\alpha = 0.24$ , means that all the points construct a pattern.

At the beginning phase of the exponential curve, which starts at  $Re = 25\,147$  with  $\lambda_{rmax} = -0.000\,907\,88$ , the points are loose between the points. As the  $Re$  is getting higher, the points are getting denser, means that the change in  $\lambda_{rmax}$  is

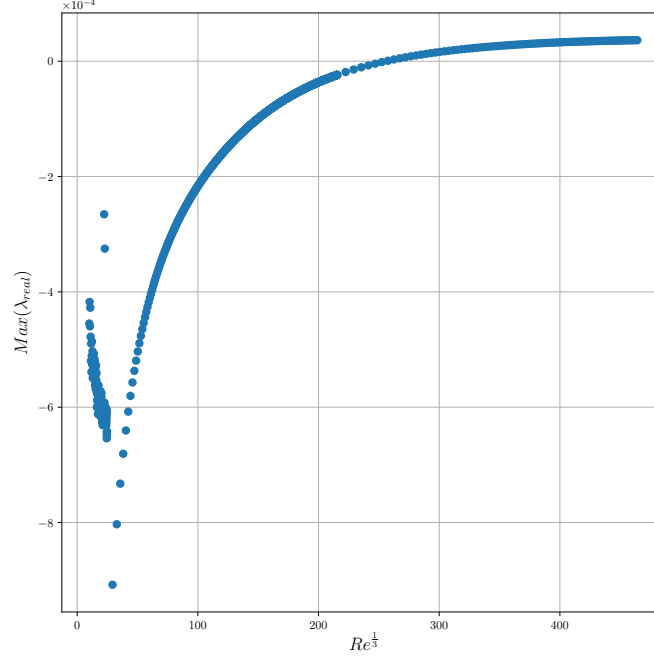


FIGURE 4.1: Data plot Reynolds number vs. Real Lambda for  $\alpha = 0.01$ ,  $Re_{crit} = 1.6 \times 10^7$

not as big as it is at the low  $Re$ . Although  $\lambda_{rmax}$  takes a wider gap again before the transition, the increase of  $\lambda_{rmax}$  is gradually lesser.

#### 4.2.2 Data Plot for Wavenumber 0.15

An examination on this second case will be done for  $\alpha = 0.15$  with the same range of  $Re$ . The data plot can be seen in Figure 4.2. Broadly speaking, the trend of the graph is increasing semi-parabolically and then slightly exponential. Within this range, the flow experiences an unstable state between  $Re = 55\,589$  and  $Re = 390\,452$ . Following this, the condition returns to the stable state ( $\lambda_{rmax}$  is negative).

At the stage of semi-parabolic curve, there is a big jump of  $\lambda_{rmax}$  value after a point at  $Re = 1.5 \times 10^4$  with a value of  $\lambda_{rmax} = -0.001\,910\,80$  to a point at  $Re = 25\,147$  with a value of  $\lambda_{rmax} = -0.000\,843\,73$ . This is happened because

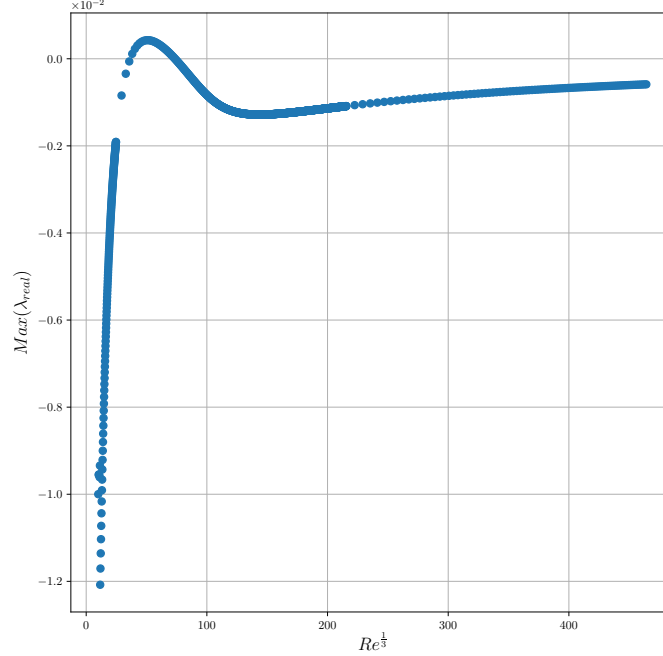


FIGURE 4.2: Data plot Reynolds number vs. Real Lambda for  $\alpha = 0.15$ ,  $Re_{crit} = 45\,442$

it is the point where the second range of  $Re$  with a different step starts. Some unordered points are still apparent on the low  $Re$ . Nevertheless, they are getting far less than that at  $\alpha = 0.01$ .

Before the slight exponential increase,  $\lambda_{rmax}$  performs a decrease from the maximum point at  $Re = 146\,916$  with  $\lambda_{rmax} = 0.000\,422\,68$  to a point at  $Re = 2\,967\,881$  with  $\lambda_{rmax} = -0.001\,282\,48$ . In spite of the fact that the second stage are increasing, it is less likely to go back to an unstable state considering that the delta between the points are getting lower.

### 4.2.3 Data Plot for Wavenumber 0.24

In this part, a data with alpha  $\alpha = 0.24$  will be examined with the same range of  $Re$ . In general, the whole trend shows almost the same plot with the previous one,

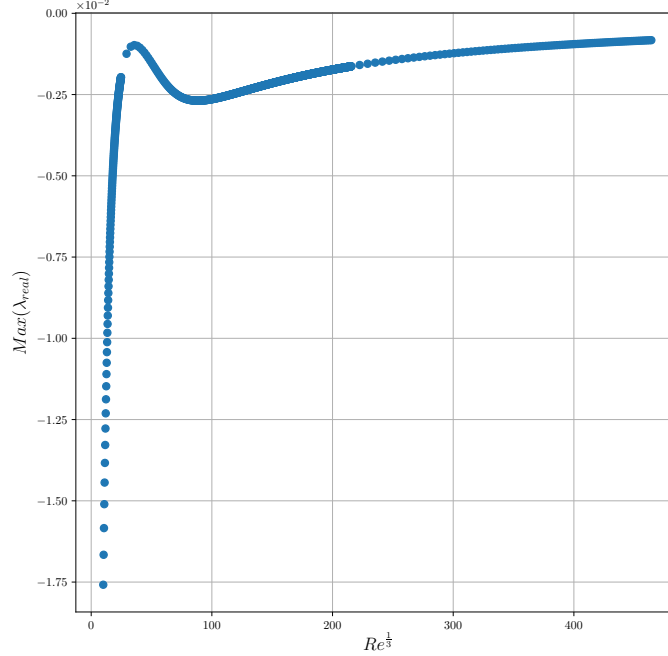


FIGURE 4.3: Data plot Reynolds number vs. Real Lambda for  $\alpha = 0.24$ , no  $Re_{crit}$

as shown in Figure 4.3. In this plot, the instability status indicates a stable state for the whole range.

Starting from this  $\alpha$ , the maximum point will be a local maximum since at the middle of the second stage, the value of  $\lambda_{rmax}$  is larger than the local maximum value. In this case, the local maximum is at  $Re = 45\,442$  with a value of  $\lambda_{rmax} = -0.000\,978\,22$ . Another point to be highlighted is that the whole range is a fully stable state.

After the local maximum, the  $\lambda_{rmax}$  drops until  $Re = 694\,873$  with a value of  $\lambda_{rmax} = -0.002\,689\,00$ . Then, it increases exponentially until the last value of Reynolds number  $Re = 1 \times 10^8$  with a value of  $\lambda_{rmax} = -0.000\,922\,94$ . Another point to be addressed is that there is no more unordered point at the lower  $Re$ , as previously mentioned.

#### 4.2.4 Data Plot for All Wavenumbers

This section will be discussing the Figure 4.4 which plots the entire range of  $\alpha$  from 0.01 to 0.30. Each  $\alpha$  is distinguished by a pair of symbol and color as listed in the legend of the Figure. Overall, the plots produce a rapid-exponential increase at the beginning, and then increase progressively after a short decrease.

As discussed before, the plots show a full stable state from  $\alpha = 0.20$  to  $\alpha = -0.30$  while the condition for the  $\alpha$  less than 0.20 is stable at first, unstable for a short range of  $Re$ , and then recovers back to the stable state. Scattered points for  $\alpha$  less than 0.24 at low Reynolds number are observable as well. In terms of growth, the highest growth occurs at  $198\,155 < Re < 500\,566$  for the wavenumbers from  $\alpha = 0.10$  to  $\alpha = -0.12$

It is also clear from the graph that the  $\alpha$  affects the maximum/local maximum value quite significant. The higher the  $\alpha$ , the lower the maximum/local maximum value. The local maximum of  $\alpha = 0.30$ , denoted by purple-colored "+" sign, is the lowest value, followed by the next. However, the difference of  $\alpha$  from 0.13 to the lowest is very insignificant.

### 4.3 Stability Analysis at Complex Plane

This section will be examining the growth of eigenvalues at a specific pair of  $Re$  and  $\alpha$  on a complex plane ( $\lambda_{real}$  at  $x$ -axis and  $\lambda_{imag}$  at  $y$ -axis). The stable flow will be denoted by a negative value of  $\lambda_{real}$  while unstable condition will be indicated by a positive value of  $\lambda_{real}$ . For comparison, there will be two pairs of  $Re$  and  $\alpha$  that will be investigated.

#### 4.3.1 Stable State

For the first plot, the eigenvalues at  $Re = 8000$  and  $\alpha = 0.30$  are plotted at the complex plane, as shown in Figure 4.5. The value of  $\lambda_{rmax} = -0.00458198$ , it means that this condition maintains a stable state as there is no  $\lambda_{real}$  with a positive sign. Or, it can be said that all the  $\lambda_{real}$  lie in the left-half plane.

A STUDY OF LAMINAR-TURBULENT TRANSITION ON TWO-DIMENSIONAL  
 SUCTION BOUNDARY LAYER

---

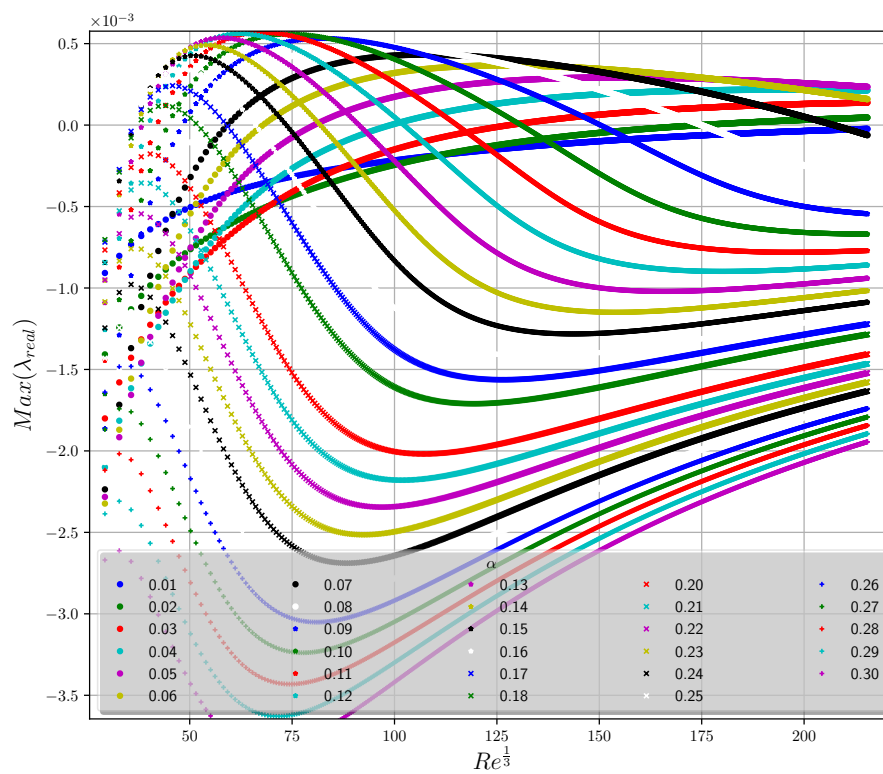


FIGURE 4.4: Data plot Reynolds number vs. Real Lambda for all wavenumbers

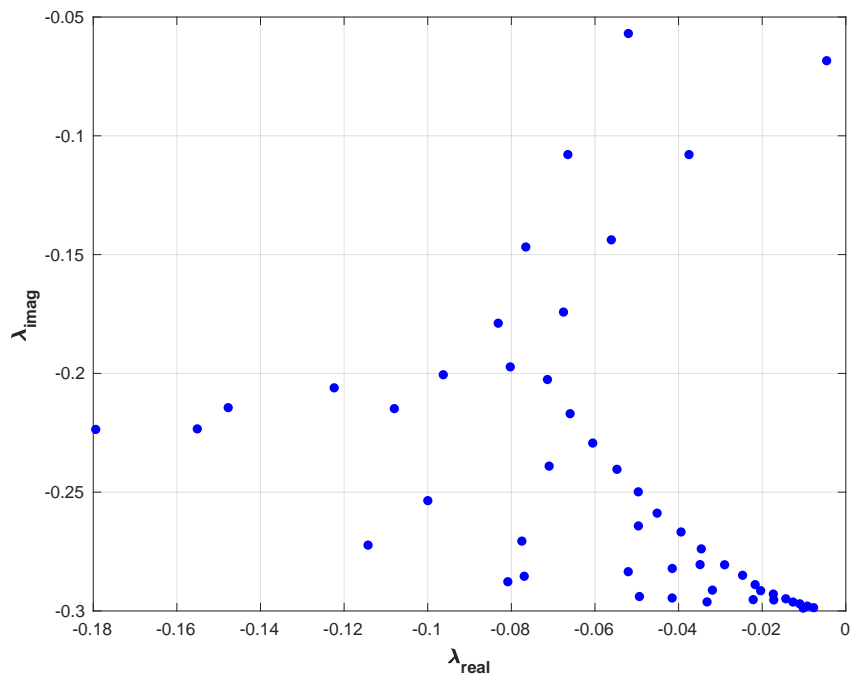


FIGURE 4.5: Eigenvalues for  $Re = 8000.0$  and  $\alpha = 0.30$  at a complex plane shows a stable state

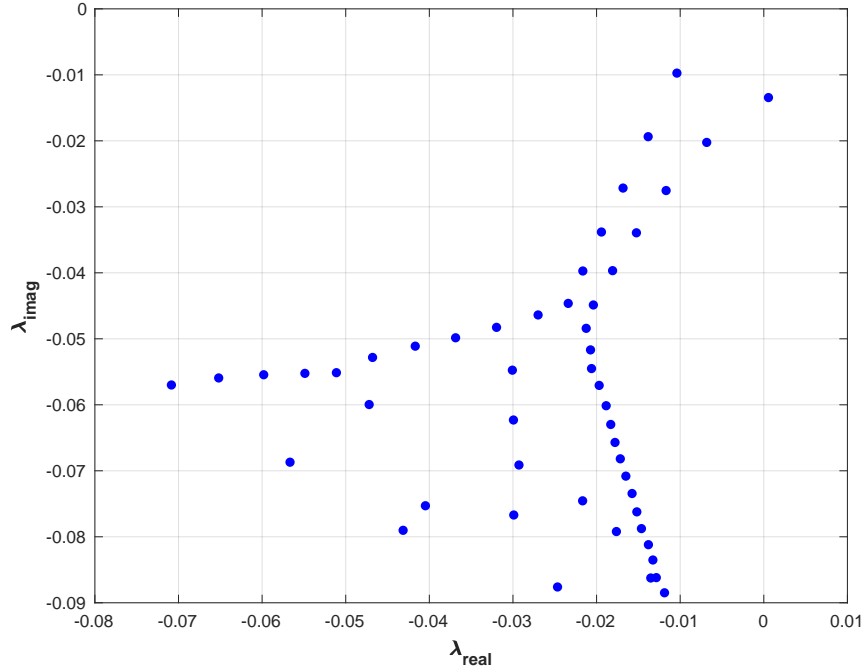


FIGURE 4.6: Eigenvalues for  $Re = 216\,000$  and  $\alpha = 0.12$  at a complex plane shows an unstable state

### 4.3.2 Unstable Condition

The next plot of eigenvalues at  $Re = 216\,000$  and  $\alpha = 0.12$  will be examined, as demonstrated in Figure 4.6. Unstable condition occurs if any of the  $\lambda_{real}$  are in the right-half plane. As can be seen from the graph, there is already one point that crosses into the right-half plane. It is the point of  $\lambda_{rmax}$  itself with a value of  $\lambda_{rmax} = 0.000\,558\,08$ . Thus, this condition experiences an unstable state.

## 4.4 The Contour of Stability

### 4.4.1 Contour Plot of The Data

This part will discuss a contour of  $\lambda_{rmax}$  in terms of the stability of the flow, as exemplified in Figure 4.7. Two variables impacts the  $\lambda_{rmax}$ , namely  $Re$  and  $\alpha$ . The

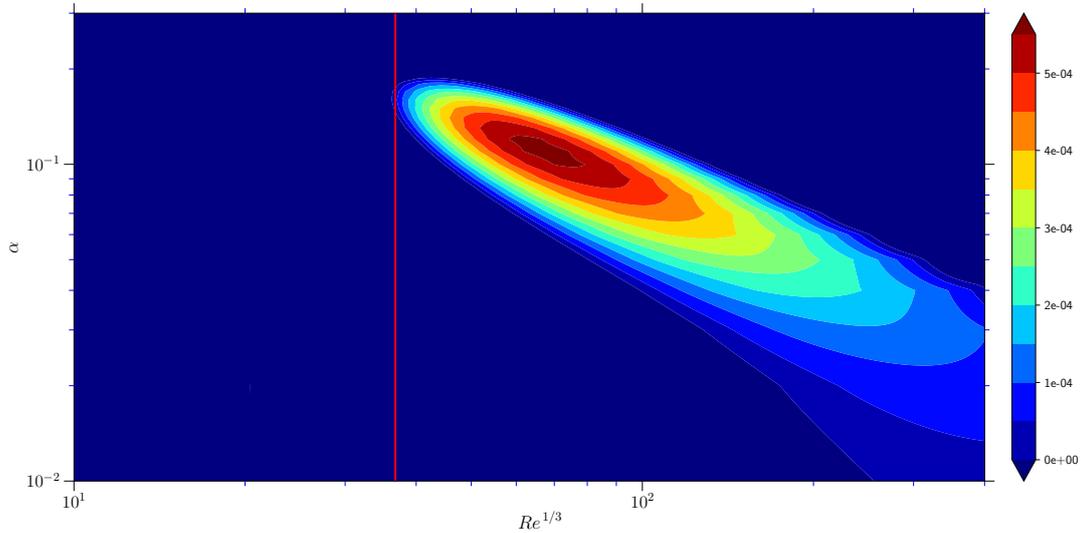


FIGURE 4.7: The contour plot of neutral stability for a viscous flow

$Re$  varies between  $1 \times 10^3$  and  $1 \times 10^8$ , while  $\alpha$  varies between 0.01 and 0.30 with a linear space of 0.01. On this study, only a viscous flow that is being analyzed.

The thumb-shaped curve is where the unstable region takes place since all the  $\lambda_{rmax}$  are positive. Inside the thumb-shaped curve, the color denotes the value of the  $\lambda_{rmax}$ . The more red the color is, the higher the  $\lambda_{rmax}$  are. Outside that region, it is stable, means that the  $\lambda_{rmax}$  are negative (the darkest blue region).

Another point to be highlighted is that there is a line which separates the stable and unstable region where the value of  $\lambda_{rmax}$  are exactly 0. That line is the so-called a neutral curve. With regard to growth of the stability, all disturbances outside the thumb-shaped curve are damped.  $Re_{crit}$  is located in which where the thumb-shaped curve protrudes (marked by red line), which occurs at approximately  $Re = 48\,000$ .

According to the Rayleigh criterion, if the profile  $U(y)$  has no point of inflection, the thumb-shaped curve vanishes at a large Reynolds number. This contour seems to have no point of inflection if the range of  $Re$  is being extended. In the opposite, if the profile  $U(y)$  has a point of inflection, the contour stays open at infinity Reynolds number (unstable until infinity).

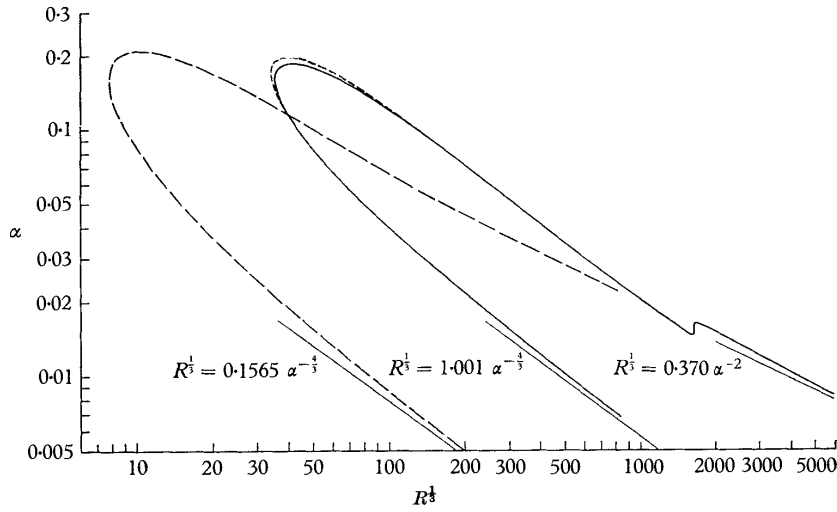


FIGURE 4.8: The curve of neutral stability for asymptotic suction profile from Hughes and Reid (Hughes & Reid, 1965)

#### 4.4.2 Comparison

The results above will be compared with the investigation conducted by Hughes and Reid (Hughes & Reid, 1965). The curve of neutral stability conducted by Hughes and Reid is shown in Figure 4.8. Two thumb-shaped curves are plotted here, the dashed line is for an inviscid flow while the solid line is for a viscous flow. To compare with the results in this study, only the viscous flow curve that will be analyzed.

The thumb-shaped curve for the viscous flow starts at Reynolds number  $Re = 6.4 \times 10^4$  and limited at  $Re = 1.25 \times 10^{11}$ . The wavenumber is ranging from  $5 \times 10^{-3}$  to  $2 \times 10^{-1}$ . Same with the preceding results, the condition outside the thumb curve is a stable state since the  $\lambda_{rmax}$  are negative. On the other hand,  $\lambda_{rmax}$  inside the thumb curve are positive, thus unstable state takes place.

It is also obvious that the  $Re_{crit}$  happens at approximately  $Re = 50\,000$ . In terms of point inflection, this viscous-affected flow seems to have no point of inflection as well, thus will disappears at high Reynolds number. In addition, the line of the curve denoted the neutral curve where  $\lambda_{rmax}$  are 0.

## CHAPTER 5

### SUMMARY, CONCLUSION, RECOMMENDATION

#### 5.1 Conclusions

Taking everything into account, the investigation on transition of a controlled suction boundary layer in temporal stability using linear stability theory has been done.

From the contour plot of  $Re$  vs  $\alpha$ , it may be concluded that the  $Re_{crit}$  brings forth at approximately  $Re = 48\,000$ , which is the value of  $Re$  where the thumb-shaped curve protrudes. In terms of stability, the darkest blue region denotes a stable condition while the others implies an unstable state. As this thumb-shaped curve seems to has no point of inflection, this curve closes at a large Reynolds number.

This determined range of Reynolds number and wavenumber as variables in the Orr-Sommerfeld Equation affects the stability of this suction flow as the base flow, on a two-dimensional streamline body, or, a flat plate to be specific. Yet, this range of Reynolds number and wavenumber still may not be able to conclude clearly regarding the transition of the flow from laminar to turbulent flow.

In terms of the execution cost, gathering the entire data require an extraordinarily high cost and time. Throughout the whole 30 wavenumbers, it takes approximately 12 hours to obtain the data for each wavenumber. This matter is as a consequence of high resolution of eigenvalues that are being acquired.

In the case of Reynolds number that is increasing within the specified range, it leads to a rapid-parabolic increase and, after a short parabolic decrease, a slight exponential increase of eigenvalues happens. The condition begins to endure a fully stable state when the wavenumber is  $\alpha > 0.18$  for all Reynolds numbers.

With respect to transition, the flow performs a recovery to a laminar flow as the delta of the eigenvalues are eventually decreasing for the whole flow at wavenumbers in range.

## 5.2 Remarks for the Future Work

For future work and development, it is recommended to analyze the spatial growth of the flow as this study only investigate the temporal growth. Also, applying other variations of base flow to study and investigate the effect to transition is also expected.

A higher resolution could be done in the future research to have a more comprehensive analysis and comparison with other studies. By this wider range of aforementioned variables, a more complete data to analyze the stability might be achieved. Moreover, an analysis in relation to the transition might be more accurate.

a higher specification of the machine could be applied to reduce the time consumption cost of the calculation. By this evaluation, it might increase the resolution of the eigenvalues as well considering the improved capability of the machine. Be that as it may, the cost to provide such machine might be a point to consider.

## References

- Abidin, M. U. (2015). *Boundary layer theory*. University Lecture.
- Anderson, J. (2016). *Fundamentals of aerodynamics*. McGraw-Hill Education.  
Retrieved from [https://books.google.co.id/books?id=\\_7VLjwEACAAJ](https://books.google.co.id/books?id=_7VLjwEACAAJ)
- Canuto, C. (2007). *Spectral methods: Evolution to complex geometries and applications to fluid dynamics*. Springer Science and Business Media.
- Hughes, T., & Reid, W. (1965). On the stability of the asymptotic suction boundary-layer profile. *Journal of Fluid Mechanics*, 23(4), 715–735.
- Islam, M. (2015, 03). *Boundary layer transition: An overview*. doi: 10.13140/RG.2.2.32152.60160
- Laminar and turbulent boundary layers*. (2005). Retrieved 2019-10-29, from [http://www-mdp.eng.cam.ac.uk/web/library/enginfo/aerothermal\\_dvd\\_only/aero/fprops/introvisc/node8.html](http://www-mdp.eng.cam.ac.uk/web/library/enginfo/aerothermal_dvd_only/aero/fprops/introvisc/node8.html)
- Laminar flow airfoil*. (2015). Retrieved 2019-11-24, from <http://www.aviation-history.com/theory/lam-flow.htm>
- Langtry, Menter, R., Florian, Likki, S., Suzen, Y., Huang, P., & Völker, S. (2006, 07). A correlation-based transition model using local variables part i: Model formulation. *ASME J. Turbomach*, 128. doi: 10.1115/1.2184352
- Mayle, R. E. (1991, 10). The 1991 IGTI Scholar Lecture: The Role of Laminar-Turbulent Transition in Gas Turbine Engines. *Journal of Turbomachinery*, 113(4), 509-536. Retrieved from <https://doi.org/10.1115/1.2929110>  
doi: 10.1115/1.2929110
- Medida, S. (2014). *Correlation-based transition modeling for external aerodynamic flows* (Unpublished doctoral dissertation).
- Nelson, D. (2018). *Laminar vs. turbulent flow*. Retrieved 2019-11-19, from <https://sciencetrends.com/the-difference-between-laminar-and-turbulent-flow/>
- On boundary layers: Laminar, turbulent and skin friction*. (2016).

- Retrieved 2019-10-29, from <https://aerospaceengineeringblog.com/boundary-layers/>
- Orszag, S. A. (1971). Accurate solution of the orrsommerfeld stability equation. *Journal of Fluid Mechanics*, 50(4), 689703. doi: 10.1017/S0022112071002842
- Reynolds, O. (1883). Xxix. an experimental investigation of the circumstances which determine whether the motion of water shall be direct or sinuous, and of the law of resistance in parallel channels. *Philosophical Transactions of the Royal Society of London*, 174, 935-982. Retrieved from <https://royalsocietypublishing.org/doi/abs/10.1098/rstl.1883.0029> doi: 10.1098/rstl.1883.0029
- Saric, W. (1986). Visualization of different transition mechanisms. *The Physics of Fluids*, 29(9), 2770-2770.
- Schlichting, H., & Gersten, K. (2016). *Boundary-layer theory*. Springer.
- Shahmohamadi, H., & Rashidi, M. M. (2017). Experimental investigation and a novel analytical solution of turbulent boundary layer flow over a flat plate in a wind tunnel. *International Journal of Mechanical Sciences*, 133, 121 - 128. Retrieved from <http://www.sciencedirect.com/science/article/pii/S0020740317304782> doi: <https://doi.org/10.1016/j.ijmecsci.2017.08.043>
- Spaulding, E. (2019, 03). Studies of boundary layer transition from laminar to turbulent.
- Stokes, G. G. (1851, 01). On the Effect of the Internal Friction of Fluids on the Motion of Pendulums. *Transactions of the Cambridge Philosophical Society*, 9, 8.
- Trefethen, L. N. (2000). *Spectral methods in matlab*. Society for Industrial and Applied Mathematics. Retrieved from <https://epubs.siam.org/doi/abs/10.1137/1.9780898719598> doi: 10.1137/1.9780898719598
- What are the navier-stokes equations?* (n.d.). Retrieved 2019-11-04, from <https://www.simscale.com/docs/content/simwiki/numerics/what-are-the-navier-stokes-equations.html>
- White, F. (2006). *Viscous fluid flow*. McGraw-Hill. Retrieved from <https://books.google.co.id/books?id=f16wPwAACAAJ>

# Appendices

## APPENDIX A

### MATLAB AND PYTHON CODES

#### A.1 Generalized Eigenvalue Problems (MATLAB)

```
1 % Function has been edited to check the reciprocal condition of the matrix
2 function e = ose_chebfun(Re_, alph_)
3     Re = Re_;
4     alph = alph_;
5     A = chebop(0, 50);
6     A.op = @(x,u) (diff(u,4)-2*alph^2*diff(u,2)+alph^4*u)/Re - ...
7         exp(-x)*1i*alph*u - 1i*alph*(1-exp(-x)).*(diff(u,2)-alph^2*u);
8     B = chebop(0, 50);
9     B.op = @(x,u) (diff(u,2) - u*alph^2);
10    A.lbc = [0; 0];
11    A.rbc = [0; 0];
12    e = eigs(A, B, 'sm');
13 end
```

#### A.2 Wavenumber Data (Python)

```
1 import numpy as np
2 import matlab.engine
3
4 # Initial values
5 # alph = 0.22 # Initial Alpha
6 # Re = 0.05e6 # Initial Reynolds number
7
8 # alphss = np.linspace(0.22, 0.3, 5).round(2)
```

A STUDY OF LAMINAR-TURBULENT TRANSITION ON TWO-DIMENSIONAL  
SUCTION BOUNDARY LAYER

---

```
9  # Ress = np.linspace(0.05e6, 2e6, 196)
10
11  Ress1 = np.linspace(1e3, 1.5e4, 150)
12  Ress2 = np.linspace(1.5e4, 1e7, 985)
13  Ress3 = np.linspace(1e7, 1e8, 90)
14
15  Ress = np.concatenate((Ress1, Ress2, Ress3))
16  #alphss = np.linspace(0.25, 0.3, 30)
17
18  alphss = [0.25, 0.26, 0.27, 0.28, 0.29, 0.3]
19
20
21  Re_steps = np.arange(Ress.shape[0])
22
23  # Starting the Matlab Engine
24  eng = matlab.engine.start_matlab()
25
26  for alph in alphss:
27      Res = []
28      alphas = []
29      lambda_rmaxs = []
30      for Re_step in Re_steps:
31          Re = Ress[Re_step]
32          status = (
33              "Re Step ="
34              + str(Re_step)
35              + " :: "
36              + "Re="
37              + str(Re)
38              + " and alph="
39              + str(alph)
40          )
41          print(status)
```

```
42     lambdas = np.array(  
43         eng.ose_chebfun(float(Re), float(alph))  
44     ) # Processing the data of eigenvalues  
45     lambda_rmax_idx = np.argmax(np.real(lambdas)) # find index of lambda_rmax  
46     lambda_rmax = lambdas[lambda_rmax_idx]  
47     print(np.real(lambda_rmax))  
48     Res = np.append(Res, Re)  
49     alphas = np.append(alphas, alph)  
50     lambda_rmaxs = np.append(lambda_rmaxs, lambda_rmax)  
51     alph_str = str("{:.3f}".format(alph))  
52     fname = "ose_re_lambda_rmax_alp_" + alph_str + ".txt"  
53     np.savetxt(  
54         fname,  
55         np.transpose([Res, alphas, np.real(lambda_rmaxs), np.imag(lambda_rmaxs)]),  
56         fmt="%.1f %.5f %.8f %.8f",  
57         delimiter=" ",  
58         header="Re      Alpha      Lambda_Re      Lambda_Imag",  
59     )
```

### A.3 Plot Each Wavenumber (Python)

```
1  import os  
2  import numpy as np  
3  import matplotlib.pyplot as plt  
4  import matplotlib  
5  matplotlib.rcParams["text.usetex"] = True  
6  
7  # folder to be processed  
8  folder = "Computation_Results/"  
9  files = os.listdir(folder)  
10 files.sort()  
11  
12 # plots folder
```

```
13 save_dir = "plots/"
14
15 # Plot for each lambda
16 for file in files:
17     alph_str = file[23:27]
18     fname = folder + file
19     data = np.genfromtxt(fname, skip_header=1)
20     Res = data[:, 0]**(1 / 3)
21     Lambda_Res = data[:, 2]
22     fig, ax = plt.subplots(figsize=(9, 9))
23     ax.plot(Res, Lambda_Res, 'o', label=alph_str)
24     ax.set_xlabel(r"$Re^{\frac{1}{3}}$", fontsize=15)
25     ax.set_ylabel(r"$Max(\lambda_{real})$", fontsize=15)
26     ax.ticklabel_format(axis="y", style="sci", scilimits=(-2, 3))
27     ax.grid("both")
28     fsavename = "Lambda_Real_VS_RealLambda_Re=" + alph_str + ".pdf"
29     plt.savefig(save_dir + fsavename, dpi=600)
30 plt.show()
```

## A.4 Plot Each Wavenumber (Python)

```
1 import os
2 import numpy as np
3 import matplotlib.pyplot as plt
4 import matplotlib
5 matplotlib.rcParams["text.usetex"] = True
6
7 # folder to be processed
8 folder = "Computation_Results/"
9 files = os.listdir(folder)
10 files.sort()
11
12 # plots folder
```

A STUDY OF LAMINAR-TURBULENT TRANSITION ON TWO-DIMENSIONAL  
SUCTION BOUNDARY LAYER

---

```
13 save_dir = "plots/"
14
15 markers = [
16     'bo',
17     'go',
18     'ro',
19     'co',
20     'mo',
21     'yo',
22     'ko',
23     'wo',
24     'b*',
25     'g*',
26     'r*',
27     'c*',
28     'm*',
29     'y*',
30     'k*',
31     'w*',
32     'bx',
33     'gx',
34     'rx',
35     'cx',
36     'mx',
37     'yx',
38     'kx',
39     'wx',
40     'b+',
41     'g+',
42     'r+',
43     'c+',
44     'm+',
45     'y+',
```

A STUDY OF LAMINAR-TURBULENT TRANSITION ON TWO-DIMENSIONAL  
SUCTION BOUNDARY LAYER

---

```
46     'k+',
47     'w+',
48 ]
49
50 fig, ax = plt.subplots(figsize=(9, 9))
51
52 n = 0
53 # Plot for each lambda
54 for file in files:
55     alph_str = file[23:27]
56     fname = folder + file
57     data = np.genfromtxt(fname, skip_header=1)
58     Res = data[:, 0]**(1 / 3)
59     Lambda_Res = data[:, 2]
60     ax.plot(Res, Lambda_Res, markers[n], markersize=3, label=alph_str)
61     n += 1
62 ax.set_xlabel(r"$Re^{\frac{1}{3}}$", fontsize=15)
63 ax.set_ylabel(r"$Max(\lambda_{real})$", fontsize=15)
64 ax.ticklabel_format(axis="y", style="sci", scilimits=(-2, 3))
65 ax.grid("both")
66 leg = plt.legend(loc='best',
67                 ncol=5,
68                 mode="expand",
69                 shadow=True,
70                 fancybox=True,
71                 title=r"$\alpha$")
72 leg.get_frame().set_alpha(0.5)
73 plt.savefig(save_dir + "Lambda_Real_VS_Re_All_Lambda.pdf", dpi=600)
74 plt.show()
```

## APPENDIX B

### EIGENVALUES DATA

#### B.1 Alpha = 0.01

#	Re	Alpha	Lambda_Re	Lambda_Imag
1000.0	0.01000	-0.00045487	-0.00996997	
1094.0	0.01000	-0.00041738	-0.00997242	
1187.9	0.01000	-0.00045974	-0.00996982	
1281.9	0.01000	-0.00042739	-0.00997191	
1375.8	0.01000	-0.00047772	-0.00996860	
1469.8	0.01000	-0.00051968	-0.00996603	
1563.8	0.01000	-0.00048970	-0.00996795	
1657.7	0.01000	-0.00053877	-0.00996473	
1751.7	0.01000	-0.00051103	-0.00996650	
1845.6	0.01000	-0.00048607	-0.00996809	
1939.6	0.01000	-0.00052629	-0.00996561	
2033.6	0.01000	-0.00050296	-0.00996710	
2127.5	0.01000	-0.00054916	-0.00996407	
2221.5	0.01000	-0.00052688	-0.00996550	
2315.4	0.01000	-0.00050638	-0.00996681	
2409.4	0.01000	-0.00054500	-0.00996442	
2503.4	0.01000	-0.00052538	-0.00996567	
2597.3	0.01000	-0.00050715	-0.00996684	
2691.3	0.01000	-0.00055031	-0.00996402	
2785.2	0.01000	-0.00053250	-0.00996516	
2879.2	0.01000	-0.00051583	-0.00996623	
2973.2	0.01000	-0.00055254	-0.00996396	
3067.1	0.01000	-0.00053630	-0.00996500	

A STUDY OF LAMINAR-TURBULENT TRANSITION ON TWO-DIMENSIONAL  
SUCTION BOUNDARY LAYER

---

3161.1	0.01000	-0.00052101	-0.00996598
3255.0	0.01000	-0.00056185	-0.00996332
3349.0	0.01000	-0.00054673	-0.00996429
3443.0	0.01000	-0.00053242	-0.00996520
3536.9	0.01000	-0.00056759	-0.00996304
3630.9	0.01000	-0.00055350	-0.00996394
3724.8	0.01000	-0.00054011	-0.00996479
3818.8	0.01000	-0.00052736	-0.00996561
3912.8	0.01000	-0.00056582	-0.00996310
4006.7	0.01000	-0.00055309	-0.00996391
4100.7	0.01000	-0.00054094	-0.00996469
4194.6	0.01000	-0.00057440	-0.00996263
4288.6	0.01000	-0.00056233	-0.00996340
4382.6	0.01000	-0.00059997	-0.00996094
4476.5	0.01000	-0.00058789	-0.00996171
4570.5	0.01000	-0.00057630	-0.00996245
4664.4	0.01000	-0.00056517	-0.00996316
4758.4	0.01000	-0.00059766	-0.00996117
4852.3	0.01000	-0.00058656	-0.00996188
4946.3	0.01000	-0.00057587	-0.00996256
5040.3	0.01000	-0.00061193	-0.00996021
5134.2	0.01000	-0.00060119	-0.00996089
5228.2	0.01000	-0.00059083	-0.00996155
5322.1	0.01000	-0.00058082	-0.00996219
5416.1	0.01000	-0.00057116	-0.00996280
5510.1	0.01000	-0.00056182	-0.00996340
5604.0	0.01000	-0.00059246	-0.00996152
5698.0	0.01000	-0.00058309	-0.00996212
5791.9	0.01000	-0.00057402	-0.00996269
5885.9	0.01000	-0.00060802	-0.00996047
5979.9	0.01000	-0.00059886	-0.00996106
6073.8	0.01000	-0.00058998	-0.00996162
6167.8	0.01000	-0.00058136	-0.00996217

A STUDY OF LAMINAR-TURBULENT TRANSITION ON TWO-DIMENSIONAL  
SUCTION BOUNDARY LAYER

---

6261.7 0.01000 -0.00057299 -0.00996270  
6355.7 0.01000 -0.00060244 -0.00996090  
6449.7 0.01000 -0.00059403 -0.00996144  
6543.6 0.01000 -0.00058585 -0.00996196  
6637.6 0.01000 -0.00057789 -0.00996246  
6731.5 0.01000 -0.00061027 -0.00996035  
6825.5 0.01000 -0.00060222 -0.00996086  
6919.5 0.01000 -0.00059437 -0.00996136  
7013.4 0.01000 -0.00058674 -0.00996184  
7107.4 0.01000 -0.00057930 -0.00996232  
7201.3 0.01000 -0.00057205 -0.00996278  
7295.3 0.01000 -0.00060001 -0.00996107  
7389.3 0.01000 -0.00059269 -0.00996153  
7483.2 0.01000 -0.00058555 -0.00996199  
7577.2 0.01000 -0.00061662 -0.00995996  
7671.1 0.01000 -0.00060937 -0.00996042  
7765.1 0.01000 -0.00060230 -0.00996087  
7859.1 0.01000 -0.00059540 -0.00996131  
7953.0 0.01000 -0.00058865 -0.00996174  
8047.0 0.01000 -0.00058206 -0.00996216  
8140.9 0.01000 -0.00057562 -0.00996257  
8234.9 0.01000 -0.00060236 -0.00996093  
8328.9 0.01000 -0.00059584 -0.00996134  
8422.8 0.01000 -0.00058947 -0.00996175  
8516.8 0.01000 -0.00061920 -0.00995980  
8610.7 0.01000 -0.00061272 -0.00996022  
8704.7 0.01000 -0.00060637 -0.00996062  
8798.7 0.01000 -0.00060016 -0.00996101  
8892.6 0.01000 -0.00062649 -0.00995941  
8986.6 0.01000 -0.00062020 -0.00995981  
9080.5 0.01000 -0.00061405 -0.00996020  
9174.5 0.01000 -0.00060802 -0.00996058  
9268.5 0.01000 -0.00060211 -0.00996095

## Turnitin Report

# STUDY OF LAMINAR-TURBULENT TRANSITION ON TWO-DIMENSIONAL SUCTION BOUNDARY LAYER

## ORIGINALITY REPORT

21%

SIMILARITY INDEX

11%

INTERNET SOURCES

9%

PUBLICATIONS

15%

STUDENT PAPERS

## PRIMARY SOURCES

1

[es.scribd.com](https://es.scribd.com)

Internet Source

2%

2

Submitted to RMIT University

Student Paper

2%

3

Submitted to Technische Universiteit Delft

Student Paper

1%

4

[www.docme.ru](http://www.docme.ru)

Internet Source

1%

5

[www.simscale.com](http://www.simscale.com)

Internet Source

1%

6

Submitted to Imperial College of Science,  
Technology and Medicine

Student Paper

1%

7

Submitted to Universiti Teknologi MARA

Student Paper

1%

8

Submitted to Higher Education Commission  
Pakistan

Student Paper

1%

9	<a href="http://dl.samegp.com">dl.samegp.com</a> Internet Source	<1%
10	Ernst Heinrich Hirschel, Jean Cousteix, Wilhelm Kordulla. "Three-Dimensional Attached Viscous Flow", Springer Nature, 2014 Publication	<1%
11	<a href="http://www.sgu.ac.id">www.sgu.ac.id</a> Internet Source	<1%
12	Submitted to University of Birmingham Student Paper	<1%
13	Submitted to Coventry University Student Paper	<1%
14	Submitted to University of South Africa Student Paper	<1%
15	<a href="http://www.slideshare.net">www.slideshare.net</a> Internet Source	<1%
16	Submitted to University of Sheffield Student Paper	<1%
17	<a href="http://www.chebfun.org">www.chebfun.org</a> Internet Source	<1%
18	Submitted to University of Johannesburg Student Paper	<1%
19	Submitted to University of Strathclyde Student Paper	<1%

20	Submitted to University College London Student Paper	<1 %
21	Lloyd N. Trefethen. "14. Fourth-Order Problems", Society for Industrial & Applied Mathematics (SIAM), 2000 Publication	<1 %
22	D. Arnal, G. Casalis. "Laminar-turbulent transition prediction in three-dimensional flows", Progress in Aerospace Sciences, 2000 Publication	<1 %
23	Submitted to The University of Manchester Student Paper	<1 %
24	Shibayama, . "Review of Fundamental Fluid Mechanics", Advanced Series on Ocean Engineering, 2008. Publication	<1 %
25	<a href="http://elib.uni-stuttgart.de">elib.uni-stuttgart.de</a> Internet Source	<1 %
26	Submitted to Emirates Aviation College, Aerospace & Academic Studies Student Paper	<1 %
27	Submitted to Preston College Student Paper	<1 %
28	<a href="http://www.sharesearch.me">www.sharesearch.me</a> Internet Source	<1 %

29

[digitalcommons.fiu.edu](https://digitalcommons.fiu.edu)

Internet Source

<1%

---

30

Robert Edward Mayle. "The 1991 IGTI Scholar Lecture: The Role of Laminar-Turbulent Transition in Gas Turbine Engines", *Journal of Turbomachinery*, 1991

Publication

<1%

---

31

[pervata.es](https://pervata.es)

Internet Source

<1%

---

32

Submitted to Cardiff University

Student Paper

<1%

---

33

Lecture Notes in Computational Science and Engineering, 2012.

Publication

<1%

---

34

A. J. Colley. "An experimental study of boundary-layer transition over a rotating, compliant disk", *Physics of Fluids*, 1999

Publication

<1%

---

35

[mafiadoc.com](https://mafiadoc.com)

Internet Source

<1%

---

36

Submitted to University of Huddersfield

Student Paper

<1%

---

37

Pijush K. Kundu, Ira M. Cohen, David R. Dowling. "Instability", Elsevier BV, 2016

Publication

<1%

---

38

[pss-gitlab.math.univ-paris-diderot.fr](https://pss-gitlab.math.univ-paris-diderot.fr)

Internet Source

<1%

---

39

Numerical Python, 2015.

Publication

<1%

---

40

Submitted to University of Mauritius

Student Paper

<1%

---

41

Submitted to Kingston University

Student Paper

<1%

---

42

Submitted to Taylor's Education Group

Student Paper

<1%

---

43

[tlmerrill.pbworks.com](https://tlmerrill.pbworks.com)

Internet Source

<1%

---

44

[kaizenha.com](https://kaizenha.com)

Internet Source

<1%

---

45

Submitted to University of Cape Town

Student Paper

<1%

---

46

[pt.scribd.com](https://pt.scribd.com)

Internet Source

<1%

---

47

Submitted to Blackpool and The Fylde College,  
Lancashire

Student Paper

<1%

---

48

[wbabin.net](https://wbabin.net)

Internet Source

<1%

---

49	<a href="https://matplotlib.org">matplotlib.org</a> Internet Source	<1%
50	Submitted to University of Nottingham Student Paper	<1%
51	Submitted to Southern Business School Student Paper	<1%
52	George Chatzigeorgiou, Nicolas Charalambakis, Yves Chemisky, Fodil Meraghni. "Continuum Mechanics and Constitutive Laws", Elsevier BV, 2017 Publication	<1%
53	Submitted to University of West London Student Paper	<1%
54	<a href="https://wikimili.com">wikimili.com</a> Internet Source	<1%
55	Submitted to Cranfield University Student Paper	<1%
56	Submitted to Aviation Management College Student Paper	<1%
57	Submitted to King Abdullah University of Science and Technology (KAUST) Student Paper	<1%
58	Submitted to Universiti Teknologi Malaysia Student Paper	<1%

59	<a href="http://www.iranpejohesh.com">www.iranpejohesh.com</a> Internet Source	<1%
60	<a href="http://robotsforex.net">robotsforex.net</a> Internet Source	<1%
61	L. L. Bonilla, A. Glavan, A. Marquina. "Wavelength selection of rippling patterns in myxobacteria", Physical Review E, 2016 Publication	<1%
62	Hiroshi Niino. "A Weakly Non-linear Theory of Barotropic Instability", Journal of the Meteorological Society of Japan. Ser. II, 1982 Publication	<1%
63	<a href="http://www.iuli.ac.id">www.iuli.ac.id</a> Internet Source	<1%
64	<a href="http://archive.org">archive.org</a> Internet Source	<1%
65	<a href="http://hdl.handle.net">hdl.handle.net</a> Internet Source	<1%
66	Submitted to National Institute of Technology Warangal Student Paper	<1%
67	<a href="http://b-ok.xyz">b-ok.xyz</a> Internet Source	<1%
68	Submitted to Universitas Islam Indonesia Student Paper	<1%

---

69	<a href="http://www.smmlab.it">www.smmlab.it</a> Internet Source	<1%
70	M. Turkyilmazoglu, N. Uygun. "Direct Spatial Resonance in the Compressible Boundary Layer on a Rotating-disk", Theoretical and Computational Fluid Dynamics, 2006 Publication	<1%
71	<a href="http://repositories.lib.utexas.edu">repositories.lib.utexas.edu</a> Internet Source	<1%
72	<a href="http://www.answers.com">www.answers.com</a> Internet Source	<1%
73	Submitted to Universiti Malaysia Perlis Student Paper	<1%
74	<a href="http://worldwidescience.org">worldwidescience.org</a> Internet Source	<1%
75	<a href="http://eprints.uthm.edu.my">eprints.uthm.edu.my</a> Internet Source	<1%
76	Submitted to Queensland University of Technology Student Paper	<1%
77	International Journal of Numerical Methods for Heat & Fluid Flow, Volume 25, Issue 3 (2015) Publication	<1%
78	Submitted to University Der Es Salaam Student Paper	<1%

---

---

79

[wwwme.nchu.edu.tw](http://wwwme.nchu.edu.tw)

Internet Source

<1%

---

80

MARKUS HÖGBERG, DAN S. HENNINGSON.  
"Linear optimal control applied to instabilities in  
spatially developing boundary layers", Journal of  
Fluid Mechanics, 2002

Publication

<1%

---

81

Cousteix, J.. "Shock layers and boundary layers  
in hypersonic flows", Progress in Aerospace  
Sciences, 1994

Publication

<1%

---

82

Submitted to University of Central England in  
Birmingham

Student Paper

<1%

---

83

[etd.uum.edu.my](http://etd.uum.edu.my)

Internet Source

<1%

---

84

Kazem Hejranfar, Mahya Hajihassanpour.  
"Chebyshev collocation spectral lattice  
Boltzmann method for simulation of low-speed  
flows", Physical Review E, 2015

Publication

<1%

---

85

Submitted to University of KwaZulu-Natal

Student Paper

<1%

---

86

[bmcmeginformdecismak.biomedcentral.com](http://bmcmeginformdecismak.biomedcentral.com)

Internet Source

<1%

---

87

Submitted to University of Central Florida

Student Paper

&lt;1%

88

[www.pvamu.edu](http://www.pvamu.edu)

Internet Source

&lt;1%

89

Submitted to American University of Athens

Student Paper

&lt;1%

90

Submitted to University of New South Wales

Student Paper

&lt;1%

91

Nikolay Ivanov Kolev. "Multiphase Flow Dynamics 3", Springer Science and Business Media LLC, 2012

Publication

&lt;1%

92

Chanjuan Yao, Botong Li, Xinhui Si, Yahui Meng. "On fluid flow and heat transfer of turbulent boundary layer of pseudoplastic fluids on a semi-infinite plate", Physics of Fluids, 2020

Publication

&lt;1%

93

Dept. Earth Sys Sci. Tech., Interdis. Grad Sch Engg Sci, Kyushu. "Fluid Dynamics for Global Environmental Studies", Springer Science and Business Media LLC, 2017

Publication

&lt;1%

94

YANBAO MA, XIAOLIN ZHONG. "Receptivity of a supersonic boundary layer over a flat plate. Part 1. Wave structures and interactions",

&lt;1%

## Journal of Fluid Mechanics, 2003

Publication

95

Submitted to University of Oxford

Student Paper

<1%

96

[repository.uinjkt.ac.id](http://repository.uinjkt.ac.id)

Internet Source

<1%

97

FRANZ DURST, BÜLENT ÜNSAL. "Forced laminar-to-turbulent transition of pipe flows", *Journal of Fluid Mechanics*, 2006

Publication

<1%

98

[digitalcommons.njit.edu](http://digitalcommons.njit.edu)

Internet Source

<1%

99

"Modeling and Computation of Boundary-Layer Flows", Springer Science and Business Media LLC, 2005

Publication

<1%

100

Submitted to Indian Institute of Technology, Madras

Student Paper

<1%

101

Submitted to University of Leicester

Student Paper

<1%

102

Jimmy Philip, Michael Karp, Jacob Cohen. "Streak instability and generation of hairpin-vortices by a slotted jet in channel crossflow: Experiments and linear stability analysis", *Physics of Fluids*, 2016

<1%

---

103	<b>Submitted to Middle East Technical University</b> Student Paper	<1%
104	<b>Submitted to University of Warwick</b> Student Paper	<1%
105	<b>Isom H. Herron. "The Orr–Sommerfeld Equation on Infinite Intervals", SIAM Review, 1987</b> Publication	<1%
106	<b>"Tubes, Sheets and Singularities in Fluid Dynamics", Springer Nature, 2002</b> Publication	<1%
107	<b>Thermal-Hydraulic Analysis of Nuclear Reactors, 2015.</b> Publication	<1%
108	<b>A. L. Uribe, H. Klahr, Th. Henning. "ACCRETION OF GAS ONTO GAP-OPENING PLANETS AND CIRCUMPLANETARY FLOW STRUCTURE IN MAGNETIZED TURBULENT DISKS", The Astrophysical Journal, 2013</b> Publication	<1%

---

Exclude quotes      Off  
Exclude bibliography      On

Exclude matches      Off

## Curriculum Vitae



---

Basic Information	
Name	Lutfi Muzzaki Khairullah
Place of Birth	Bontang, Kalimantan Timur
Date of Birth	04, 24, 1997
Address	Perumahan Foresta Cluster Studento, BSD City

---

Year	Education
2015 - present	International University Liaison Indonesia (IULI)
2012 - 2015	SMA Yayasan Pupuk Kaltim
2009 - 2012	SMP Yayasan Pupuk Kaltim
2003 - 2009	SD 1 Yayasan Pupuk Kaltim

---

Year	Seminars & Workshops
2017	Aeroleadership Camp 2017
2017	Workshop on Structural Health Monitoring for Aircraft Structure
2017	Technology and Culture Facing the Global Market
2017	The Understanding of Airmanship and Its Relation to Flight Safety
2016	An Introduction to Maintenance and Structure Repair of Aircraft
2015	Modern Metro Systems for Environmental Friendly Megacities

---

Year	Work Experiences
2020	UI/UX Developer - PT. Aviasi Jaya Indonesia
2019	Internship Product Design and Development - GASI GmbH
2017	On Job Training - Sriwijaya Air

---